"Propagation of non-diffracting beams in turbulent media"

Thesis submitted to the Medicine school of University of Crete in partial fulfillment of the requirements for the Degree Master of Science in Optics and Vision

ANASTASIA GIANNAKOPOULOU

BSc in Mathematics

Approved by:

1) Papazoglou Dimitris
Assistant Professor, Materials Science and Technology
Department, UoC
2) Taroudakis Michael
Professor, Mathematics Department UoC
3) Tzortzakis Stelios
Researcher B, IESL, FORTH

<u>Acknowledgements</u>

The completion of this thesis signals the end of my two-year studies for the acquisition of the Master Degree of Science in Optics and Vision at the University of Crete. At the same time, it gives me the opportunity to express my gratitude to all those people who supported me throughout my studies, as well as to those who helped me, both directly and indirectly, to complete my thesis.

First of all, I would like to thank my supervisor, Prof. Dimitrios Papazoglou, for his continuous guidance throughout the conduction of my study. It was a great honor for me to work with Prof. Papazoglou, who apart from being an excellent scientist, distinguished by his special ability to communicate his knowledge to his students; he is also a man of rare quality. In effect, through his profound knowledge, his inspiring comments and his useful advice, he offered me great guidance and at the same time he stimulated my interest in this research area. I personally thank him for his constant willingness to offer me his help and support, which made a great contribution to my paper. Indeed, this cooperation of ours has provided me with invaluable knowledge, which will be proved of great importance for the continuation of my studies.

I am also grateful to Dr. Michael Taroudakis for the guidance and precious advice that he offered me throughout my studies, as well as for always being patient with me and good-humored.

I would also like to thank Dr. Stelios Tzortzakis for his assistance and his cooperation towards the completion of this thesis.

Special thanks go to my tutors of the Postgraduate MSc Programme "Optics and Vision" -and especially to Dr. Aristophanes Pallikaris and to Dr. Harilaos Ginis- for the precious knowledge they offered me and for their constant willingness to help me.

I would also like to thank the PhD candidates Mr. Paris Panagiotopoulos, Ms. Loukia Leonidou, Mr. Konstantinos Gourgoulias and Ms. Rigoula Karagkouni-Siaplaoura and also the Master student Clement Paradis for their crucial assistance during the conduction of my dissertation.

Many thanks go to my colleagues and friends from the Master Programme, with whom I shared moments of stress and anxiety, but mostly moments of great joy. I would also like to thank my colleagues from IESL for all that time we spent studying together, and especially Mr. Evangello Marakis for all his support. It goes without saying that I am grateful to all my friends for their patience, support and love throughout my studies all these years.

Last but not least, I would like to express my deep gratitude to my family, my parents Georgios and Sofia, and especially to my brother Antonis, for their love and their support, and for all the great things they have offered me and the sacrifices they have made throughout all these years of my studies, not only until now but in the future as well.

<u>TABLE OF CONTENTS</u>

Abstract

Chapters:

<u>Abstract</u>

The advent of powerful and stable laser sources has recently revived the interest for optical free space communication systems. Besides the progress in this field a major problem that still has to be solved is the effect of air turbulence on signal quality. A straightforward method to overcome the deteriorating effects of turbulence is to use non-diffracting beams that in principle have the ability to self heal. In this thesis we numerically study the propagation of non-diffracting beams, Airy and Bessel, in turbulent media. Their propagation is compared with the propagation of plane waves, Gaussian beams and a recently presented type of accelerating self focusing beams the Airy Ring beam. Our simulations were preformed both in 1+1D by numerically solving the paraxial approximation of the wave equation and in 2+1D using a slit step technique involving the propagation of the angular spectrum and random phase screens to represent the turbulence. Our simulations indicate that in general turbulence can severely affect the propagation of non-diffracting beams since it scrabbles the wavefront in a continuous and distributed way that cannot be balanced by the self healing action. On the other hand under some conditions, Airy Beams can be better when propagating in turbulence from Gaussian Beams while Bessel Beams had almost the same response to turbulence as Gaussian Beams. Interestingly, Airy Ring Beams seem to be quite promising in propagating though high turbulence in comparison to all other beam types used in our simulations.

1. Introduction

In recent years, and after the invention of Ruby laser in 1960, there has been a growing interest in the subject of free space optical communication techniques. Especially at the beginning of research scientists thought that it would help space-based applications, but the lack of proper systems in laser technology delayed this development. Research in free optical communications began a cycle of declining interest and funding different from time to time[1].

At late 90's, free space laser communication come back to the surface, in order to cover the great demand for high bandwidths communications. The explosion of internet was a reason for the creation of this great demand. This period of time, the establishment of optical fiber communications, led scientists to span these efficient components in Free Space Optical (FSO) systems, but a drawback was that it was costly.

Nowadays, difficulties and the high cost of laying a network of optical fibers in urban areas, created a need of modulation and propagation of optical signals over a line-of sight path (Figure 1). Additionally, the great advantages in the sector of communications made them one of the hottest technologies of this decade. These advantages are rapidly deploy-ability, support for high bandwidth transmissions, high security, the ability to extend the reach of the optical fiber backbone and the use in physical disaster recovery situations (valuable for quick reconstruction of communications in areas with damages in copper wires, optical fibers and/or radio frequency antennas).
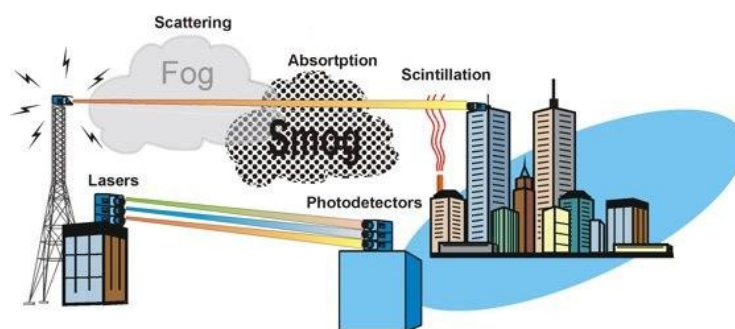
Figure 1: Representation of a FSO system
(http://zyumed.com/modules/com_ccboard/free-space-optics-1688.html)

Although FSO are promising, there are components that could not be neglected such as atmospheric turbulence, aerosols and molecular attenuation. These

components generate problems to the propagation of beams in atmosphere and scientists are trying to overcome them.

In this thesis, the problem of propagation in atmospheric turbulence will be investigated numerically. The atmospheric turbulence and the propagation of different types of beams will be simulated. The purpose of this study is to find a more "proper" beam from the laser beam, in order to improve the signal that finally reaches from the transmitter to the receiver in FSO systems.

The types of beams that will be simulated numerically and compared for 1+1dimensions and for 2+1 dimensions are:

- 1+1 Dimensions
    o Gaussian Beams
    o Airy Beams
    o 2 Colliding Airy Beams
- 2+1 Dimensions
    o Gaussian Beams
    o Airy Beams
    o Bessel Beams
    o Airy Ring Beams (accelerating auto focusing beams)

Initially paraxial approximation will be described and the connection of it with beams. Also the parameters of propagation of beams and the numerical modeling approach for 1+1 and 2+1 dimensions will be described. And finally the results and further research will be presented.

At this direction was the theoretical approach for evolution of Airy Beams in turbulence given by Chu[2] . He found that when the value of a in an Airy Beam is small, the Airy Beam can be more resilient against turbulence perturbations. Additionally, Gu's[3] simulations for 4 Airy Beams that collapse show that Airy Beams parameters should be chosen appropriately in order Airy beams' intensity peaks to retain their displacements. Another work of Gu[4] for pseudo-Bessel Beams in atmospheric turbulence results that with proper manipulation of the parameters; pseudo-Bessel Beams are more "proper" for propagation in turbulence than Gaussian Beams. These previous works and the new type of beams, Airy Ring Beams, led to the result that non-diffracting beams are challenging for research and their behavior in turbulence should be checked.

2. Paraxial approximation

2.1 Wave Equation

Maxwell's equations for a region with no charge or current (p=0, j=0) are, in differential form:

$$\overline{\nabla} \cdot \overline{D} = 0 \tag{1}$$

$$\overline{\nabla} \cdot \overline{B} = 0 \tag{2}$$

$$\overline{\nabla} \times \overline{E} = -\frac{\partial \overline{B}}{\partial t} \tag{3}$$

$$\overline{\nabla} \times \overline{H} = \frac{\partial \overline{D}}{\partial t} \tag{4}$$

There are two variables that describe the electric properties of the electromagnetic field E and D, and also two variables for the magnetic properties of the field H and B (this is necessary when some materials are present with oriented electric and magnetic dipoles). If the electric dipole density is denoted by P and the magnetic dipole density by M, then the following definitions for D and B can be used (for isotropic materials):

$$\overline{D} = \varepsilon(x, y, z) \cdot \overline{E} \tag{5}$$

$$\overline{B} = \mu \cdot \overline{H} \tag{6}$$

where ε is the electric permeability and μ is the magnetic permeability

From equations (5), (6), it is taken at equations (3), (4):

$$\overline{\nabla} \times \overline{E} = -\mu \cdot \frac{\partial \overline{H}}{\partial t} \tag{7}$$

$$\overline{\nabla} \times \overline{H} = \varepsilon \cdot \frac{\partial \overline{E}}{\partial t} \tag{8}$$

From Equation 7 it is taken:

$$\overline{\nabla} \times \left(\overline{\nabla} \times \overline{E} \right) = \overline{\nabla} \times \left(\frac{\partial \overline{B}}{\partial t} \right) = \overline{\nabla} \times \left(\mu \cdot \frac{\partial \overline{H}}{\partial t} \right) = -\mu \cdot \frac{\partial}{\partial t} \left(\overline{\nabla} \times \overline{H} \right) = -\varepsilon \cdot \mu \frac{\partial^2 \overline{E}}{\partial t^2} \Rightarrow$$

$$\overline{\nabla} \cdot \left(\overline{\nabla} \cdot \overline{E} \right) - \overline{\nabla}^2 \overline{E} = -\varepsilon \cdot \mu \frac{\partial^2 \overline{E}}{\partial t^2} \tag{9}$$

From equation (5) it can be assumed (for weak perturbations) that:

$$\overline{\nabla} \cdot \left(\overline{\nabla} \cdot \overline{E} \right) \cong 0 \qquad (10)$$

Finally from equations (9) and (10) it is taken:

$$\boxed{\overline{\nabla}^2 \overline{E} - \varepsilon \cdot \mu \cdot \frac{\partial^2 \overline{E}}{\partial t^2} = 0 \qquad (11)}$$

So Maxwell equations lead directly $\overline{E}$ and $\overline{B}$ satisfying the wave equation for which the solutions are linear combinations of plane waves travelling at the speed

$$\upsilon = \frac{1}{\sqrt{\varepsilon \cdot \mu}} \qquad (12).$$

2.2 Paraxial approximation

If the Laplacian operator is expanded, it is obtained:

$$\overline{\nabla}^2 = \left[\frac{\partial^2}{\partial x^2} + \frac{\partial^2}{\partial y^2} + \frac{\partial^2}{\partial z^2} \right] = \left[\overline{\nabla}_\perp{}^2 + \frac{\partial^2}{\partial z^2} \right] \qquad (13)$$

where $\overline{\nabla}_\perp{}^2 \equiv \dfrac{\partial^2}{\partial x^2} + \dfrac{\partial^2}{\partial y^2}$ is the transverse part of the Laplacian equation. From equations (11), (12), (13), it is taken

$$\left[\overline{\nabla}_\perp{}^2 + \frac{\partial^2}{\partial z^2} \right] \cdot \overline{E} - \frac{1}{\upsilon^2} \cdot \frac{\partial^2 \overline{E}}{\partial t^2} = 0 \qquad (14)$$

In paraxial approximation the complex magnitude of the electric field $\overline{E}(x, y, z, t)$ becomes

$$E(x, y, z, t) = f(x, y, z) \cdot e^{i \cdot k_0 \cdot n_0 \cdot z - i \cdot \omega \cdot t} \qquad (15)$$

where n_0 is the mean value of the refractive index, k_0 is the free space wavenumber related to the free space wavelength λ_0, ω is the angular frequency and c is the speed of light in vacuum and the complex valued function $f(x, y, z)$ is a slowly varying function of z on a scale of $1/k_0 \cdot n_0$. The phase of f describes the departure of the phase front of the wave from that of a plane wave.

And so the longitudinal derivative $\dfrac{\partial^2}{\partial z^2}$ is equal to:

$$\frac{\partial^2 E}{\partial z^2} = \frac{\partial^2 f}{\partial z^2} \cdot e^{i \cdot k_0 \cdot n_0 \cdot z - i \cdot \omega \cdot t} + 2 \cdot i \cdot k_0 \cdot n_0 \cdot \frac{\partial f}{\partial z} \cdot e^{i \cdot k_0 \cdot n_0 \cdot z - i \cdot \omega \cdot t} - k_0^{\,2} \cdot n_0^{\,2} \cdot f \cdot e^{i \cdot k_0 \cdot n_0 \cdot z - i \cdot \omega \cdot t} \quad (16)$$

Additionally:

$$\frac{\partial^2 E}{\partial t^2} = \frac{\partial^2 \left(f \cdot e^{i \cdot k_0 \cdot n_0 \cdot z - i \cdot \omega \cdot t} \right)}{\partial t^2} = -\omega^2 \cdot f \quad (17)$$

Substituting (15), (16) and (17) into equation (14) it is obtained the following:

$$\left[\overline{\nabla}_\perp^{\,2} + \frac{\partial^2}{\partial z^2} \right] \cdot f(x, y, z) \cdot e^{i \cdot k_0 \cdot n_0 \cdot z - i \cdot \omega \cdot t} + \frac{\omega^2}{\upsilon^2} \cdot e^{i \cdot k_0 \cdot n_0 \cdot z - i \cdot \omega \cdot t} = 0 \Rightarrow (16) \Rightarrow$$

$$\left(\frac{\partial^2 f}{\partial x^2} + \frac{\partial^2 f}{\partial y^2} \right) \cdot e^{i \cdot k_0 \cdot n_0 \cdot z - i \cdot \omega \cdot t} + \frac{\partial^2 f}{\partial z^2} \cdot e^{i \cdot k_0 \cdot n_0 \cdot z - i \cdot \omega \cdot t} + 2 \cdot i \cdot k_0 \cdot n_0 \cdot \frac{\partial f}{\partial z} \cdot e^{i \cdot k_0 \cdot n_0 \cdot z - i \cdot \omega \cdot t} -$$

$$-k_0^{\,2} \cdot n_0^{\,2} \cdot f \cdot e^{i \cdot k_0 \cdot n_0 \cdot z - i \cdot \omega \cdot t} + \frac{\omega^2}{\upsilon^2} \cdot f \cdot e^{i \cdot k_0 \cdot n_0 \cdot z - i \cdot \omega \cdot t} = 0 \Rightarrow$$

$$\overline{\nabla}_\perp^{\,2} f + \frac{\partial^2 f}{\partial z^2} + 2 \cdot i \cdot k_0 \cdot n_0 \cdot \frac{\partial f}{\partial z} - k_0^{\,2} \cdot n_0^{\,2} \cdot f + \frac{\omega^2}{\upsilon^2} \cdot f = 0 \quad (18)$$

The paraxial approximation places certain upper limits on the variation of the amplitude function $f(x, y, z)$ with respect to longitudinal distance z.

A variation of f can be written as: $\delta A = \frac{\partial A}{\partial z} \cdot \delta z \ll A, \delta z \sim \lambda$ (λ is the wavelength)

so that: $\frac{\partial f}{\partial z} \ll f \big/ \lambda \sim k \cdot f$ and also:

$$\frac{\partial^2 f}{\partial z^2} \ll k \cdot \frac{\partial f}{\partial z} \ll k^2 \cdot f \quad (19)$$

Because of the paraxial inequalities stated above (19), the term $\frac{\partial^2 f}{\partial z^2}$ can be neglected

in comparison to $\frac{\partial f}{\partial z}$. This yields the paraxial approximation of the wave equation

(12):

$$\overline{\nabla}_\perp^{\,2} f + 2 \cdot i \cdot k_0 \cdot n_0 \cdot \frac{\partial f}{\partial z} - k_0^{\,2} \cdot n_0^{\,2} \cdot f + \frac{\omega^2}{\upsilon^2} \cdot f = 0 \quad (20)$$

In addition: $k = \dfrac{\omega}{\upsilon} = \dfrac{\omega}{c/n} = n \cdot \dfrac{\omega}{c} = n \cdot k_0$ (where k_0 is the wavenumber of vacuum) and

so:

$$\overline{\nabla}_{\perp}^{2} f + 2 \cdot i \cdot k_0 \cdot n_0 \cdot \frac{\partial f}{\partial z} - k_0^{2} \cdot n_0^{2} \cdot f + k_0^{2} \cdot n^{2} \cdot f = 0 \Rightarrow$$

$$\overline{\nabla}_{\perp}^{2} f + 2 \cdot i \cdot k_0 \cdot n_0 \cdot \frac{\partial f}{\partial z} + k_0^{2} \left(n^{2} - n_0^{2} \right) \cdot f = 0 \Rightarrow$$

$$\overline{\nabla}_{\perp}^{2} f + 2 \cdot i \cdot k_0 \cdot n_0 \cdot \frac{\partial f}{\partial z} + k_0^{2} \cdot \left(n + n_0 \right) \cdot \left(n - n_0 \right) \cdot f = 0 \Rightarrow$$

For a small disturbance of the refractive index it is taken $n + n_0 \cong 2 \cdot n_0$. And also by setting $\Delta n \equiv n - n_0$, finally is taken the paraxial equation[5]:

$$\overline{\nabla}_{\perp}^{2} f + 2 \cdot i \cdot k_0 \cdot n_0 \cdot \frac{\partial f}{\partial z} + k_0^{2} \cdot 2 \cdot n_0 \cdot \Delta n \cdot f = 0 \qquad (21)$$

Normalized paraxial wave equation (1+1D)

In order to normalize the paraxial equation for 1+1D it is applied the following coordinate transformations (x, z coordinates):

$$\left. \begin{aligned} s &= \frac{x}{w_0} \\ \xi &= \frac{z}{w_0^{2} \cdot n_0 \cdot k_0} \\ V &= w_0^{2} \cdot k_0^{2} \cdot n_0 \cdot \Delta n \end{aligned} \right\} \Rightarrow \qquad (22)$$

$$\boxed{\frac{1}{2} \cdot \frac{\partial^{2} f}{\partial s^{2}} + i \cdot \frac{\partial f}{\partial \xi} + V \cdot f = 0 \qquad (23)}$$

Normalized paraxial wave equation (2+1D)

In order to normalize the paraxial equation it is applied the following coordinate transformations:

$$\left.\begin{array}{l} x = w_0 \cdot x' \\ y = w_0 \cdot y' \\ z = w_0^2 \cdot n_0 \cdot k_0 \cdot z' \\ V = w_0^2 \cdot k_0^2 \cdot n_0 \cdot \Delta n \end{array}\right\} \Rightarrow$$

(24)

$$\boxed{\frac{1}{2} \cdot \overline{\nabla}_\perp^2 f + i \cdot \frac{\partial f}{\partial z'} + V \cdot f = 0 \qquad (25)}$$

3. Beams

3.1 Gaussian Beams

Gaussian beams are a well-known beam of electromagnetic radiation. Their transverse electric field and intensity (irradiance) distributions can be approximated by Gaussian functions. Laser beams are a good approximation of Gaussian beams. They are a solution of paraxial approximation (Equation 25) with initial condition for 2+1 dimensions (for $E(x', y', z')$ being the complex amplitude of beam's electric field and z' being the direction of propagation):

$$E(x', y', 0) = E_0 \cdot \exp\left(-\frac{(x'^2 + y'^2)}{w_0^2}\right)$$

(26)

where E_0 is the electric field in the center of the beam and w_0 is the waist of the beam.

For a Gaussian beam, the complex electric field amplitude in homogenous medium is described by the function[6]:

$$E(x', y', z') = E_0 \cdot \frac{w_0}{w(z')} \cdot \exp\left(-i \cdot [kz' - \eta(z')] - (x'^2 + y'^2) \cdot \left[\frac{1}{w^2(z')} + \frac{i \cdot k}{2 \cdot R(z')}\right]\right)$$

(27)

where the waist, the radius of curvature, the phase term and the diffraction length, respectively, are given by:

$$w^2(z') = w_0^2 \cdot \left[1 + \left(\frac{\lambda \cdot z'}{\pi \cdot w_0^2}\right)^2\right] = w_0^2 \cdot \left[1 + \left(\frac{z'}{z_R}\right)^2\right]$$

(28)

$$R(z') = z' \cdot \left[1 + \left(\frac{\pi \cdot w_0^2}{\lambda \cdot z'}\right)^2\right] = z' \cdot \left[1 + \left(\frac{z_R}{z'}\right)^2\right]$$

(29)

$$\eta(z') = \tan^{-1}\left(\frac{\lambda \cdot z'}{\pi \cdot w_0^2}\right) = \tan^{-1}\left(\frac{z'}{z_R}\right)$$

(30)

$$z_R = \frac{\pi \cdot w_0^2}{\lambda}$$

(31).

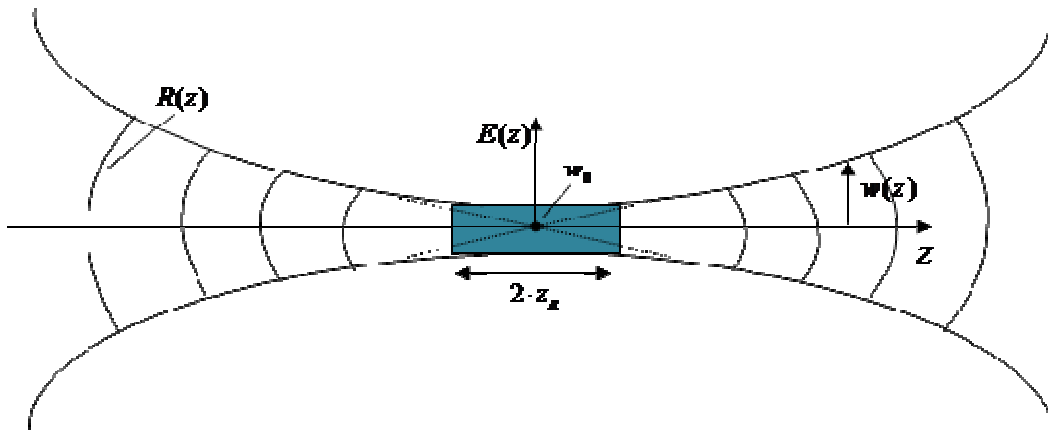The relationship between all these characteristics of a Gaussian beam is shown in Figure 2.

Figure 2: Representation of Gaussian Beam

The irradiance distribution of the Gaussian beam is given by:

$$I(x',y',z') = |E(x',y',z')|^2 = I_0 \cdot \exp\left(-\frac{2 \cdot (x'^2 + y'^2)}{w^2(z')} \right)$$

(27)

where I_0 is the irradiance in the center of the beam. The Gaussian shape is truncated at some diameter either by the internal dimensions of the laser beam or by some limiting aperture at the optical train. In order to discuss the propagation characteristics of a laser beam, it is necessary to define its diameter. There are two ways of defining its diameter, the first one is the diameter at which the beam irradiance (intensity) has fallen to $1/e^2$ (13, 5%) of its peak (waist) and the second one is the one at which the intensity of the beam has fallen to 50% of its peak. The second one is called Full Width at Half Maximum (FWHM). This is shown schematically at Figure 3.
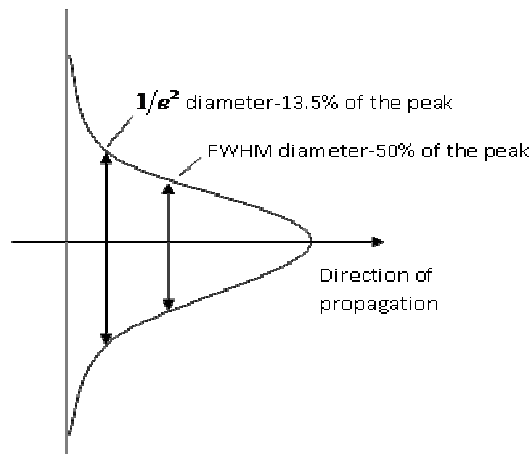

Figure 3: Diameter of a Gaussian beam

3.2 Non-diffracting and accelerating beams

The phenomenon of diffraction is a characteristic of the wave nature of light and it occurs when any wavefront is obstructed in some way. The wavefront may be corrupted in amplitude or phase because of diffraction. It has the possibility of happening anytime when a beam of light passes through an opening or aperture that is large with respect to its wavelength. According to the Huygens-Fresnel Principle[7], every point of the wavefront that is unobstructed by the hindrance serves as a source of spherical wavelets that constructively and destructively interfere with each other depending on their optical path length. This creates what is called a diffraction pattern. Diffraction causes the intensity profile of the laser (Gaussian) beam to spread out as it propagates through free space. Durnin[8,9] was the first one that pointed out that a set of solutions for the free-space scalar wave equation were "non-diffracting". Durnin entered 2D diffraction-free optical wave packets, Bessel beams, and his work gained theoretical and experimental interest and resulted to the discovery of other interesting non-diffracting solutions, Airy beams. Both types of nonspreading beams are generated from appropriate superposition of plane waves and they are beams conveying finite power (this outcome from their nondiffracting nature). This type of beams are also self-healing, which means that they can be partially obstructed at one point, but will re-form at a point further down the beam axis. In experiments of course, all nondiffracting beams are truncated by apertures, because of the extremely high energy and the space they need. As a result they seem to diffract during propagation. Nevertheless, if the geometrical size of the limiting aperture greatly exceeds the spatial features of the ideal propagation of the invariant fields, the diffraction process is decelerated over the designed propagation distance and therefore for all these reasons they are called "diffraction-free".

3.2.1 Airy Beams

The normalized paraxial equation can describe, except for Gaussian beams, a nonspreading Airy wave packet solution. The basic feature of this Airy packet is the capability to freely accelerate without including any external potential. Apart from plane waves, Airy wave packets are the only nontrivial solution of the paraxial equation that remains invariant with time. Experiments show that after Airys' beams

propagation, they retain their features, even though their truncation is exponential. Airy beams are consisting of one main lobe with maximum intensity and other smaller lobes, their propagation path is parabolic. Smaller lobes seem to supply the main lobe constantly with energy, and Airy beams accelerate throughout their propagation trajectory. This type of propagation retains over long distances despite the fact that the centroid stays constant and the phenomenon of diffraction ultimately occurs[10,11].

The initial condition for the paraxial solution (Eq.23) of Airy beam for 1+1D is:

$$f(s, \xi = 0) = Ai(s) \cdot \exp(a \cdot s)$$

(32)

where $a > 0$ is the dissipation rate. Ai is the airy function and it is defined i.e. for real values of x by the integral:

$$Ai(x) = \frac{1}{\pi} \cdot \int_0^\infty \cos\left(\frac{1}{3} \cdot t^3 + x \cdot t\right) dt$$

(33)

The initial condition for the paraxial solution (Eq.25) of Airy beam for 2+1D is:

$$f(x', y', z' = 0) = Ai(x'/x_0) \cdot Ai(y'/y_0) \cdot \exp\left(a \cdot x'/w_1\right) \cdot \exp\left(a \cdot y'/w_2\right)$$

(34)

where φ is the electric field envelope, x_0 and y_0 are arbitrary transverse scales and finally, w_1 and w_2 are the waists of the corresponding transverse scales.

For an (1+1D) Airy beam, the solution of equation (23) with initial condition equation (26) in homogenous medium (the third term of equation 23 is neglected) is described by the function:

$$f(s, \xi) = Ai\left[s - \left(\frac{\xi}{2}\right)^2\right] \cdot \exp\left(i\left(\frac{s \cdot \xi}{2}\right) - i \cdot \left(\frac{\xi^3}{12}\right)\right)$$

(35)

This mathematical relationship was stated by Berry at 1979[12].

3.2.2 Bessel Beams

The other type of non-diffracting beams is Bessel beams. Bessel beams, unlike Airy beams, are non-unique and like plane waves, they have finite energy and density but not infinite power. The ideal Bessel beam solution is given when the electric field is proportional to the zero-order Bessel function. Bessel functions of first kind $J_m(x)$ are solutions of the Bessel differential equation:

$$x^2 \cdot \frac{d^2 y}{dx^2} + x \cdot \frac{dy}{dx} + (x^2 - m^2) \cdot y = 0$$

(36)

The zero-order Bessel function $J_0(x)$ can be represented by the infinite power series:

$$J_0(x) = \sum_{i=0}^{\infty} (-1)^i \frac{\left(\frac{1}{4} \cdot x^2 \right)^i}{(i!)^2}$$

(37)

Or an integral form:

$$J_0(x) = \frac{1}{\pi} \cdot \int_0^{\pi} \exp(i \cdot x \cdot \cos \vartheta) d\vartheta$$

(38)

Consequently, zero-order Bessel function $J_0(x)$ is the initial condition for solving the paraxial equation (Eq. 25).

Bessel beams are interesting, because they have a central region that appears to overcome the effects of diffraction. When the central maximum of a zero-order Bessel beam is compared to a Gaussian beam of same size, the central maximum of the Bessel beam does not exhibit diffractive spreading.

3.3 Airy Ring Beams

Airy Ring Beams are a recently introduced type of abruptly autofocusing waves [N. K. Efremidis and D. N. Christodoulides, "Abruptly autofocusing waves," Opt. Lett. **35**, 4045-4047 (2010)., D. G. Papazoglou, N. K. Efremidis, D. N. Christodoulides, and S. Tzortzakis, "Observation of abruptly autofocusing waves," Opt. Lett. **36**, 1842-1844 (2011).]. Generally speaking, any beam with proper manipulation of the initial phase or amplitude focuses or defocuses. In some cases, for

example in medical use, it's extremely necessary for a beam to focus in a particular target, preserving low intensity before the focus. For this reason it important for medical applications to use a new category of optical beams in which the energy flows constantly and with an accelerating way accumulates at the focus point. Airy ring beams are radially symmetric waves, whose peak intensity remains constant during propagation, although, near the focal point, they autofocus and as a result their maximum intensity can abruptly increase by orders of magnitude just at the focus. In this thesis, for the 1+1D propagation, in order to present these types of beams, two Airy beams that collapse will be used. Additionally for the 2+1D propagation a radial Airy profile will be used[13,14].

The initial beam for the 1+1D will be:

$$f_0(s) = \left[Ai\left(\frac{r_0 + s}{w} \right) + Ai\left(\frac{r_0 - s}{w} \right) \right] \cdot \exp(-a \cdot s) \tag{39}$$

where Ai is the airy function (Eq.33), s is the transverse coordinate, r_0 is the radius of the beam and w is a scaling factor.

The radially symmetric Airy distribution for 2+1D is represented by:

$$f_0(s) = Ai\left(\frac{r_0 - s}{w} \right) \cdot \exp\left(a \cdot \left(\frac{r_0 - s}{w} \right) \right) \tag{40}$$

where Ai is the airy function (Eq.33), r_0 is the radius of the primary ring, w is a scaling factor and a is the exponential decaying factor.

Typical intensity profiles of all types of beams that were used are shown in Figures 4 and 5.
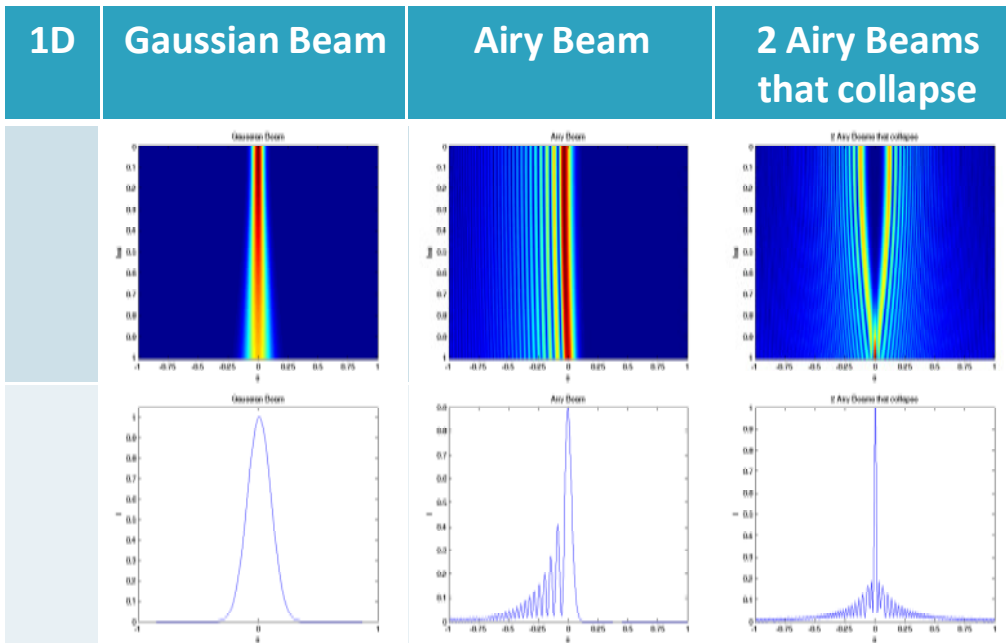
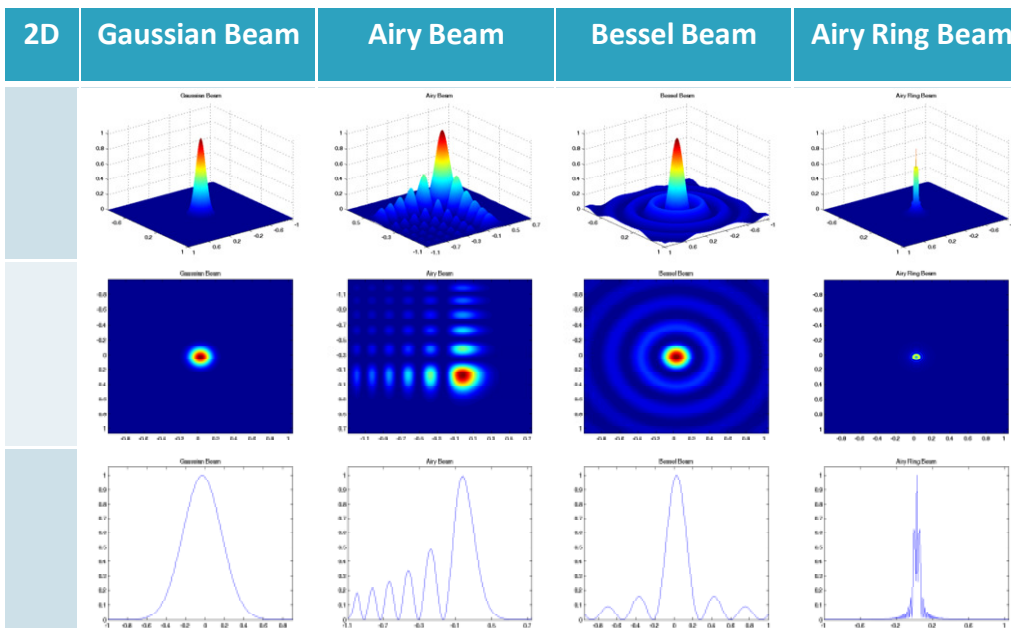Figure 4: Types of 1D beams compared in the simulations

Figure 5: Types of 2D beams compared in the simulations

4 Propagation in turbulent media

4.1 Introduction

Propagation of optical waves through the atmosphere is affected by atmospheric turbulence, scattering off aerosols, and atmospheric absorption. In this thesis will be examined the basic cause of distortion, atmospheric turbulence. Atmospheric turbulence is a result of localized variations of temperature, humidity, and pressure in the atmosphere. These variations result in localized refractive index fluctuations, where each localized area of lower or higher refractive index is known as a turbulent eddy. The refractive index of each individual eddy is not much greater than unity, but the cumulative effect of eddies over 1 km path is great.

The refractive index of air at optical frequencies is,

$$n - 1 = 77.6 \cdot \left(1 + \frac{7.52 \cdot 10^{-3}}{\lambda^2}\right) \cdot \left(\frac{P}{T}\right) \cdot 10^{-6}$$

(41)

where n is the total refractive index, λ is the wavelength in μm, P is the pressure in mbar and T is the temperature in K. At sea level, $n-1$ is typically $3 \cdot 10^4$. Humidity effects are typically neglected over land, since humidity affects the value of the refractive index by less than 1%.

In addition to energy loses associated with absorption and scattering effects and refraction-included variations of the trajectory, a beam propagating in the atmosphere also experiences amplitude and plane fluctuations due to the random space-time distribution of the refractive index are caused by disordered turbulent air mixing and, accordingly, temperature variations.

Estimates show that $1°C$ variation of the air temperature is accompanied by an order of 10^{-6} variation of the refractive index. The amplitude of the observed air-temperature fluctuations at a given point attains tenths of a degree Celsius. The period of the fluctuations varies from a few milliseconds to several seconds. The amplitude of the temperature fluctuations along horizontal paths in the atmosphere can attain several degrees for points situated at distances of the order of 10^2 to 10^3 m.

Inasmuch as the atmosphere is always turbulent, it is particularly important to study the laws by which turbulence affects the parameters of radiation, specifically in connection with the extraordinary possibilities afforded by the application of radiation

in communications systems, data transmission systems, linear and angular distance facilities, etc.

The turbulent state of the atmosphere disrupts the coherence of radiation and can, therefore, limit the capabilities of beams in devices that utilize the coherence property. Wavefront distortions induced by turbulent fluctuations of the refractive index elicit broadening of beams, random variations of the position of the beam "centroid", redistribution of the beam energy within the cross section, and related intensity fluctuations.[15]

4.2 Refractive Index fluctuations

Air movements are characterized by disordered variations of both the magnitude and the direction of velocity at any point. The result is vigorous mixing. Such motion is called turbulent, as distinct from laminar motion in which mixing does not occur and the velocity at a given point is either constant or varies in a regular fashion. The transition from laminar to turbulent motion takes place at a definite critical value of the Reynolds number:

$$\mathrm{Re} = \upsilon \cdot L / v_m \qquad (42)$$

where υ is a characteristic flow velocity, L is the characteristic space scale of the flow process and v_m is the kinematic viscosity of the fluid.

In the ground layer of the atmosphere, for a height $L = 2m$ characteristic velocities $\upsilon = 1 - 5 \, m/s$ and $v_m = 0.15 \, cm^2/s$. The Reynolds numbers have values $\mathrm{Re} = (2.5 - 7) \cdot 10^5$ i.e., are very large, and so the motion is highly turbulent.

Richardson [Reference] first developed a picture of the turbulent energy redistribution in the atmosphere. The process is shown pictorially in Figure 6, with an energy input region, inertial subrange, and energy dissipation region. The dissipation rate E is related to the velocity U_l of an eddy with characteristic length l by $U_l \approx (\mathrm{E} \cdot l)^{1/3}$. At large characteristic lengths l a portion of kinetic energy in the atmosphere is converted into turbulent energy. When the characteristic length reaches a specified outer scale length, L_0, energy begins to cascade. The energy of one eddy is

progressively redistributed into eddies of smaller scales, until eddies reach a size equal to the inner scale length, l_0. The inner scale length, or Kolmogorov microscale, is defined by: $l_0 = 7.4 \cdot (\upsilon^3/E)^{1/4}$. At the surface of Earth, l_0 is typically in the order of $4mm$ and υ is typically $0.148 \, cm^2/s$. Kolmogorov proposed that the inertial subrange, where $L_0 > l > l_0$, turbulence is isotropic and may be transferred from eddy to eddy without loss. When the diameter of a decaying eddy reaches l_0, the energy of the eddy is dissipated at heat energy through viscosity process.
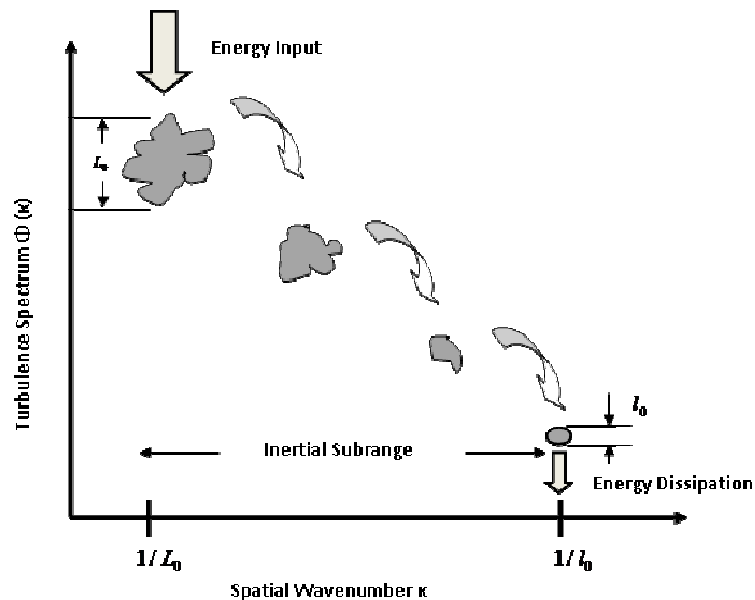

Figure 6: Depiction of the process of turbulent decay, showing the energy cascade and subsequent division of turbulent eddies in the atmosphere [Reference]

Turbulent air motion represents a set of vortices of various diameters, from extremely large with a characteristic scale L_0 to extremely small with a scale l_0 The value of L_0 is determined by the space scale of the flow on the whole and is called the outer turbulence scale. Under the influence of inertial forces, large vortices break up into smaller ones. This cascade process of the breakup of vortices continuous until the Reynolds numbers attain values of unit order and viscous forces begin to play a decisive role in comparison with the inertial forces. The scale l_0 is customarily referred

to as the inner turbulence scale. The internal of scales between L_0 and l_0 is called inertial in connection with the fact that vortices falling within this interval of scales behave mainly in accordance with the action of the inertial forces. Vortices with scale $r \leq l_0$ belong to the viscous dissipation interval.

The cascade mechanism of transfer of kinetic energy from larger vortices to smaller ones is constantly maintained in the atmosphere through external sources of energy, which feed the overall flow of moving air. The dissipation of kinetic energy is realized in the smallest vortices. Therefore the turbulence characteristics are divided according to the size of the eddy or blob into three regions:

a) **Input range** (eddy size> L_0). The energy is introduced into the turbulence in this range of eddy sizes due to wind shear and temperature gradient. In general, the turbulence is anisotropic in this range. The spectrum in this range depends on how the turbulence is created for the particular case, and thus there is no general formula describing the turbulence characteristics in this range. The referred spectrum in this section is described analytically below.

b) **Inertial subrange** (L_0 >eddy size> l_0). In this range, the kinetic energy of the eddies dominates over the dissipation due to the viscosity, and the turbulence is essentially isotropic. The spectrum is proportional to $\kappa^{-11/3}$, where $\kappa = \dfrac{2 \cdot \pi}{(eddy\ size)}$.

c) **Dissipation range** (l_0 >eddy size). In this range, the dissipation of energy due to viscosity dominates over the kinetic energy, and therefore, the spectrum is extremely small.

The scale L_0, as mentioned, is determined by the total flux. Thus, the value of L_0 in the ground layer is of the order of the height of the point of observation, and even though larger vortices may be present in the flow, they are perceived in the case merely as variations of the total flux. The scale l_0 is of the order of $1-10 mm$ near the earth's surface (Figure 7, Figure 8).
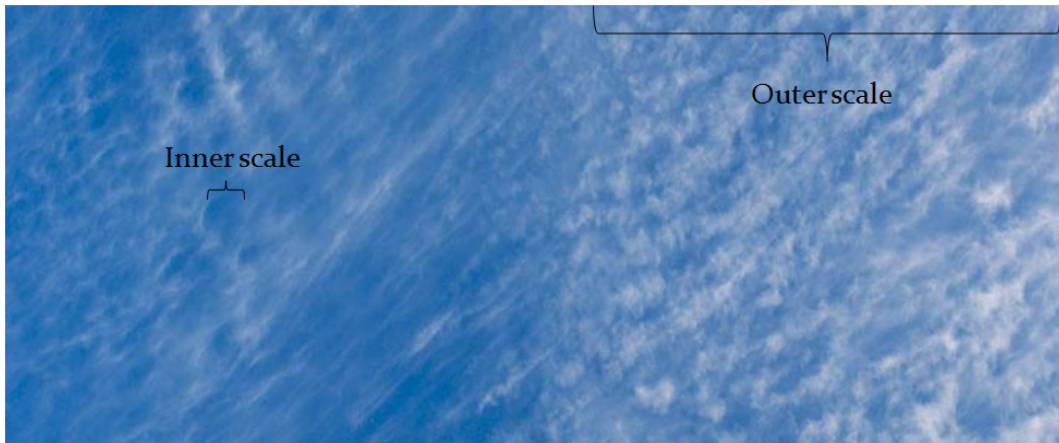
Figure 7: Turbulent eddies showing inner and outer scales
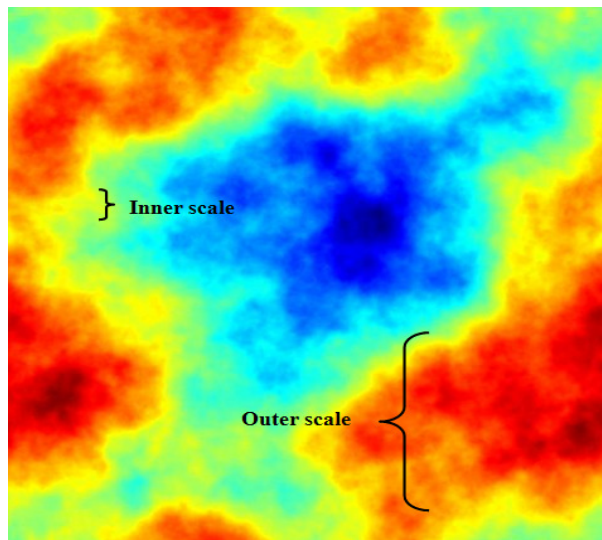(http://www.handprint.com/ASTRO/seeing1.html)

Figure 8: Turbulent eddies showing inner and outer scales

The refractive index $n(\bar{r})$ in a turbulent medium is a random function depending on the position $\bar{r}$ and time. The spatial structure of the refractive index can be described by the correlation function $B_n(\bar{r}, \bar{r}') = \left\langle \tilde{n}(\bar{r})\tilde{n}(\bar{r}') \right\rangle$. The subscript n denotes that the correlation function describes the refractive index fluctuations. Here, $\tilde{n} = n - \left\langle n \right\rangle$ is the deviation of the mean value. In turbulence theory the structure function $D_n(\bar{r}, \bar{r}')$ is usually used as $D_n(\bar{r}, \bar{r}') = \left\langle (\tilde{n} - \tilde{n}')^2 \right\rangle$. These two functions are related by the formula:

$$D_n(\bar{r}, \bar{r}') = B_n(\bar{r}, \bar{r}) + B_n(\bar{r}', \bar{r}') - 2 \cdot B_n(\bar{r}, \bar{r}') \ . \tag{43}$$

In case of statistical homogeneity all the statistical characteristics do not depend on the position, but only on the relative position. In this case $D_n(\bar{r} - \bar{r}') = 2 \cdot \left[B_n(0) - B_n(\bar{r} - \bar{r}') \right]$, where $D_n(\bar{r} - \bar{r}') = D_n(\bar{r}, \bar{r}')$, $B_n(\bar{r} - \bar{r}') = B_n(\bar{r}, \bar{r}')$. The function $D_n(\bar{r}, \bar{r}')$ can be considered as isotropic for small enough values of the vector $\bar{r} - \bar{r}'$. This means that D_n does not depend on the direction of $\bar{r} - \bar{r}'$ but only on its value $\rho = |\bar{r} - \bar{r}'|$ (Figure 9).

The function $D_n(\rho)$ is quadratic for $\rho \ll l_0$. The inner scale l_0 shows the scale of smallest inhomogeneities. For $\rho \ll l_0$, $n(r)$ is a random linear function. For very large Reynolds numbers the structure function $D_n(\rho)$ has, in the range $l_0 \ll \rho \ll L_0$, the form:

$$D_n(\rho) = C_n^2 \rho^{2/3}, \ l_0 \ll \rho \ll L_0 \tag{44}$$

where l_0 is the inner scale of turbulence, L_0 is the outer scale of turbulence and C_n^2 is the refractive-index constant. For $\rho \gg L_0$ the structure function $B_n(\rho) \cong 0$ and the structure function $D_n(\rho) \cong 2 \cdot \sigma_n^2 = const.$. Here, $\sigma_n^2 = \left\langle \tilde{n}^2 \right\rangle$ is the variance of the refractive index. The inhomogeneities with the scale $\rho \gg L_0$ are statistically independent.

Near the Earth's surface, the random medium may be treated as isotropic and it can be considered that $B_n(\bar{\rho}) \to B_n(\rho)$. In spherical coordinates the three dimensional Fourier transform for the spatial covariance is:

$$
\begin{aligned}
B_n(\rho) &= \int d^3\bar{\kappa} \cdot \exp\left(i \cdot \bar{\kappa} \cdot \bar{\rho}\right) \cdot \Phi_n(\bar{\kappa}) = \\
&\int_{-\infty}^{\infty} \int_0^{\pi} \int_0^{2\pi} d\kappa \cdot \kappa^2 \sin(\theta) d\theta d\varphi \cdot \kappa \cdot \exp\left(i \cdot \bar{\kappa} \cdot \bar{\rho}\right) \cdot \Phi_n(\bar{\kappa}) = \\
&4 \cdot \pi \cdot \int_0^{\infty} d\kappa \cdot \kappa^2 \cdot \Phi_n(\kappa) \cdot \frac{\sin(\kappa \cdot \rho)}{\kappa \cdot \rho}
\end{aligned}
\tag{45}
$$

where $\Phi_n(\kappa)$ is the isotropic and homogenous spectrum of turbulence and κ is the transverse wavenumber. A Fourier integral can also be derived from the description of the spatial covariance of the Fourier transform for the structure function related to an isotropic and homogenous turbulence spectrum:

$$D_n(\rho) = 8 \cdot \pi \cdot \int_0^\infty d\kappa \cdot \kappa^2 \cdot \Phi_n(\kappa) \cdot \left(1 - \frac{\sin(\kappa \cdot \rho)}{\kappa \cdot \rho} \right) \tag{46}$$

Equations (44) and (46) describe the refractive index structure function and the can be compared in order to determine the wavenumber power spectrum.

$$C_n^2 \cdot \rho^{2/3} = 8 \cdot \pi \cdot \int_0^\infty d\kappa \cdot \kappa^2 \cdot \Phi_n(\kappa) \cdot \left(1 - \frac{\sin(\kappa \cdot \rho)}{\kappa \cdot \rho} \right) \tag{47}$$

$\Phi_n(\kappa)$ is an equivalent representation of $D_n(\rho)$ in the inverse space.[16]

In stratified media (atmosphere, ocean) L_0 may depend on the direction. The function can be matched in the points $\rho = l_0$ and $\rho = L_0$. If $D_n(\rho) = M \cdot \rho^2$ for $\rho < l_0$ and $D_n(\rho) = C_n^2 \cdot \rho^{2/3}$ for $\rho > l_0$, matching in the point $\rho = l_0$ leads to the formula $M = C_n^2 \cdot l_0^{-4/3}$. In the same way for the point $\rho = L_0$, it is obtained that $C_n^2 \cdot L_n^{2/3} = 2 \cdot \sigma_n^2$. Thus the representation of $D_n(\rho)$ in different ranges has the form:

$$D_n(\rho) = \begin{cases} C_n^2 \cdot l_0^{-4/3} \cdot \rho^2 & for \quad \rho \ll l_0, \\ C_n^2 \cdot \rho^{2/3} & for \quad l_0 \ll \rho \ll L_0, \\ C_n^2 \cdot L_0^{2/3} & for \quad \rho \gg L_0. \end{cases} \tag{48}$$
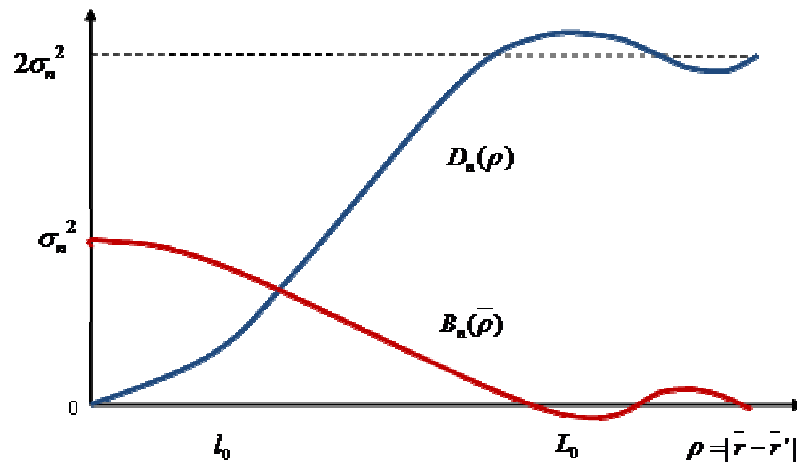
Figure 9: Typical behavior of the correlation B_n (ρ) and the structure D_n (ρ) functions of the refractive index in a turbulent medium [Reference]

The typical value of l_0 in the atmosphere is $1cm$. The value of L_0 in the atmosphere depends on the elevation. For the boundary layer of the atmosphere $L_0 = 0.4 \cdot z$, z being the height. For the free atmosphere L_0 is about $100m$ in the vertical direction and several kilometers in the horizontal direction. In the ionosphere is the order of several tens in centimeters.

Physically, the refractive index structure constant C_n^2 is a measurement of the strength of fluctuations in the refractive index. Values of C_n^2 typically range from $10^{-17} m^{-2/3}$ or less for conditions of "weak" turbulence and up to $10^{-13} m^{-2/3}$ or more when turbulence is "strong"[17] In this thesis weak turbulence is considered for $10^{-18} m^{-2/3}$ and strong turbulence for $10^{-15} m^{-2/3}$. The direct relationship between refractive index fluctuations and potential temperature fluctuations is:

$$C_n^2 = 79.06 \cdot \left(\frac{P}{T^2} \right) C_\theta^2 \cdot 10^{-6}$$

(49)

where C_θ^2 is the structure constant parameter of the potential temperature fluctuations.

In this thesis turbulence near surface, from ground to several tens of meters, is examined. Although in astronomical seeing, it is necessary to examine different layers of atmosphere, figure 10 describes how turbulence is affected in higher layers of

atmosphere in relation to $C_n{}^2$. Meteorological studies and predictions are vital for astronomical seeing, figure 11 depicts the evolution of optical turbulence in La Palmas as provided by the weather forecast.[18,19]
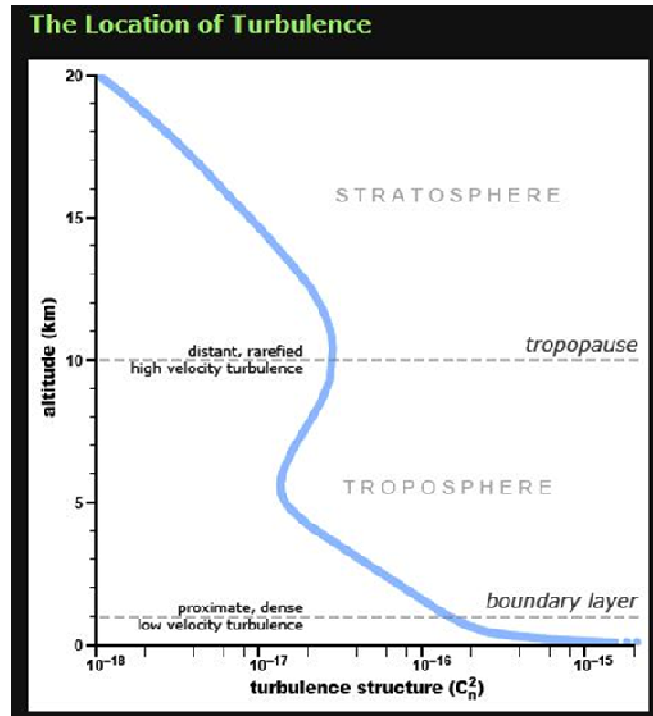
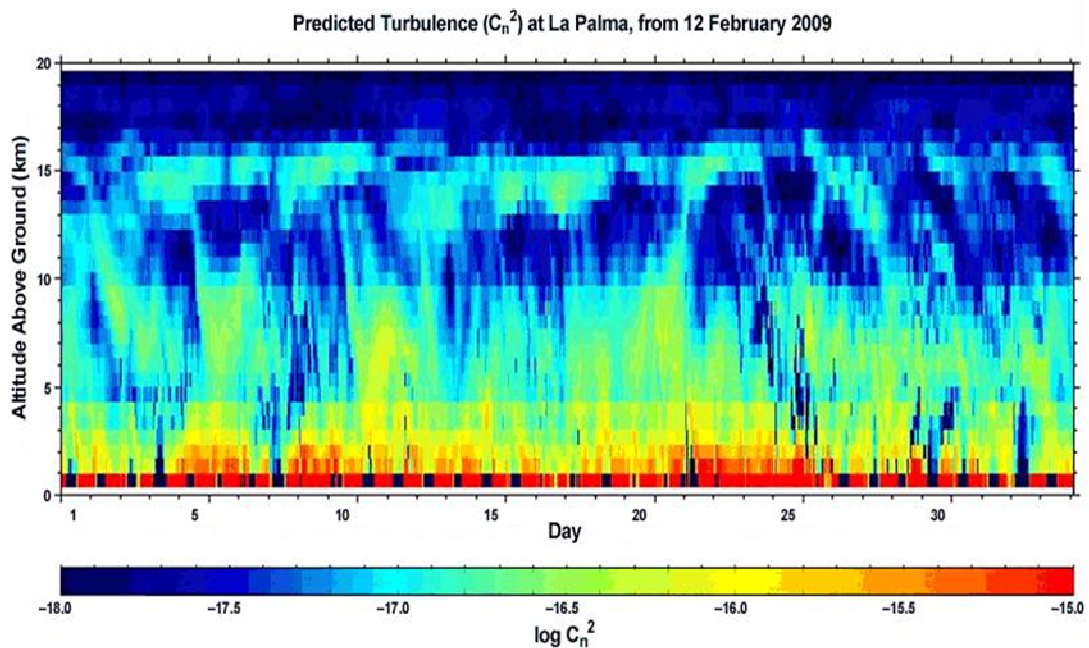Figure 10: Strength of turbulence in relation to altitude [Reference]

Figure 11: Evolution of optical turbulence-strength $C_n{}^2$ profiles as a function of altitude. The higher values of turbulence are denoted with red color and lower values with blue [Reference]

4.3 Power spectrum models

4.3.1 Kolmogorov spectrum

For optical wave propagation, refractive index fluctuations are caused almost exclusively by small fluctuations in temperature. That is, variations in humidity and pressure can usually be neglected. It is generally accepted, therefore, that the functional form of the spatial spectrum of refractive-index fluctuations is the same as that for temperature and, further that temperature fluctuations obey the same spectral laws as velocity fluctuations. The power spectral density for refractive-index fluctuations over the subrange is defined by:

$$\Phi_n(\kappa) = 0.033 \cdot C_n^{\,2} \cdot \kappa^{-11/3},$$
$$\frac{1}{L_0} << \kappa << \frac{1}{l_0} \qquad\qquad (50)$$

This equation is the Kolmogorov power-law spectrum. This spectrum model is theoretically valid only over the inertial sub-range $\frac{1}{L_0} << \kappa << \frac{1}{l_0}$. To justify its use in certain calculations over all wave numbers, it ordinary assumed that the outer scale is infinite $(L_0 = \infty)$ and the inner scale is negligibly small $(l_0 = 0)$. However, extending the validity of the equation to all wave numbers may lead to divergent integrals in some cases. Some care must therefore be exercised in the use of this spectrum model.[20]

4.3.2 Karman spectrum

Other spectrum models have been proposed for making calculations when inner scale and (or) outer scale effects cannot be ignored. The extension of the power law spectrum into the dissipation range $\kappa > 1/l_0$ requires the introduction of a function that essentially truncates the spectrum at high wave numbers. A Gaussian function was suggested for this reason and as a result the von Karman spectrum was taken and it is the following:

$$\Phi_n(\kappa) = 0.033 \cdot C_n^{\,2} \cdot \exp\left[-\left(\frac{\kappa \cdot l_0}{5.92}\right)^2\right] \cdot \left(\kappa^2 + \left(\frac{1}{L_0}\right)^2\right)^{-11/6}$$
$$(51)$$

In the inertial range, it is reduced to the Kolmogorov power-law spectrum defined above. In Figure 12, the two spectrums of turbulence are plotted for comparison.[21]
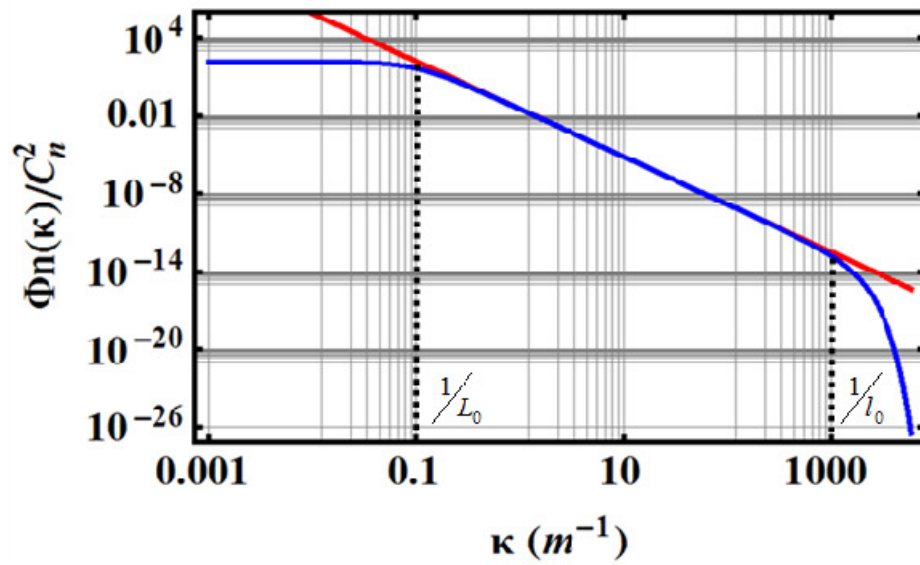

Figure 12: Kolmogorov and von Karman spectrums for turbulence

5 Numerical approaches for 1+1D propagation

5.1 Numerical solution of paraxial equation (Initial and Boundary conditions)

In order to calculate numerically propagation of the different types of beams, the paraxial equation (Eq.23 and Eq.25) can be solved numerically (Appendix B). This matter can easily be done in 1+1D simulations (Eq.23), but in 2+1D simulations, it is not so efficient, because it is computationally intensive.

The differential equation of the propagation in 1+1D is:

$$\frac{1}{2} \cdot \frac{\partial^2 f}{\partial s^2} + i \cdot \frac{\partial f}{\partial \xi} + V \cdot f = 0 \tag{52}$$

where:

$$s = \frac{x}{w_0}$$

$$\xi = \frac{z}{w_0^2 \cdot n_0 \cdot k_0}$$

$$V = w_0^2 \cdot k_0^2 \cdot n_0 \cdot \Delta n \tag{53}$$

ξ is the direction of propagation and s is the transverse coordinate of the beam. The propagation distance for all the simulations is $10km$ and s ranges from $-20cm$ to $20cm$. Three types of beams are manipulated for 1+1D propagation in this thesis. Periodic boundary conditions are used in all simulations. The initial conditions for Gaussian, Airy and two Airy Beams that collapse are successively:

$$f_0(s, \xi = 0) = \exp(-s^2) \tag{54}$$

where $w_0 = 5cm$ and $z_R = \dfrac{\pi \cdot w_0^2}{\lambda} = 10km$. For Airy Beams:

$$f_0(s, \xi = 0) = Ai\left(\sqrt{2 \cdot \log 2} \cdot (2.28/2) \cdot s\right) \cdot \exp(a \cdot s) \tag{55}$$

where $a = 0.1$ and for the two Airy Beams that collapse:

$$f_0 = \left[Ai\left(\frac{r_0 + s}{w}\right) + Ai\left(\frac{r_0 - s}{w}\right) \right] \cdot \exp(-a \cdot s) \tag{56}$$

where $a = 0.1$, $r_0 = 2$ and $w = 0,466m$. The number of the sampling points that was used was 400 for the transverse coordinate and 100 for the direction of propagation. Gaussian Beams have the same waist as the main lobe of the compared Airy Beams. The irradiance of Beams propagating without turbulence is depicted in Figure 13.
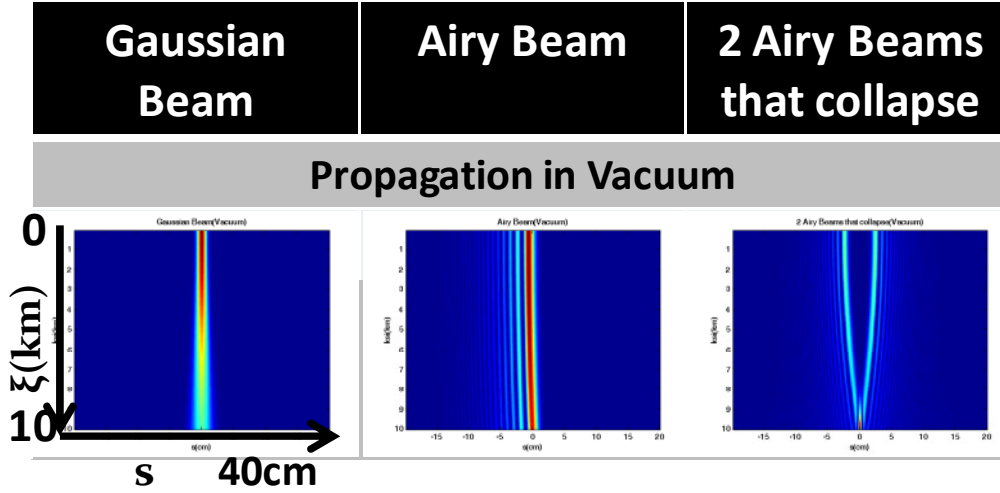

Figure 13: Irradiance of Beams in 1+1D propagation in vacuum

      The third term of Equation 52 refers to the disorder. Different values of Δn can describe low and high turbulence. Regarding to the construction of the turbulent medium of propagation, it is based on the Karman spectrum (mentioned before). All parameters of Karman model are set as the 2+1D propagation that is defined below. The final values of the turbulent medium are normalized with range from -1 to +1 and after that they are multiplied with different values of Δn proportionally to the disorder that is wished. The values of Δn range from $5 \cdot 10^{-5}$ to 10^{-7}. And the desired optical potential V is estimated from the equation:

$$V = w_0^2 \cdot k_0^2 \cdot n_0 \cdot \Delta n$$

(57)

where $w_0 = \sqrt{\dfrac{\lambda \cdot z_R}{\pi}}$, $z_R = 10km$, $k_0 = \dfrac{2 \cdot \pi}{\lambda}$, $\lambda = 0,8 \cdot 10^{-6} m$ and $n_0 \cong 1$. The maximum value of the potential V for each value of Δn is shown in Table 1. The medium of propagation consists of independent random distributions, generated using the Karman spectrum, placed every $100m$ of propagation. A schematically representation is shown in Figure 14. The code for the generation of the turbulent optical medium (distribution of refractive index respective optical potential) is given in Appendix A.

Δn	$5 \cdot 10^{-5}$	10^{-5}	$5 \cdot 10^{-6}$	10^{-6}	$5 \cdot 10^{-7}$	10^{-7}
V	785	157	78.5	15.7	7.85	1.57

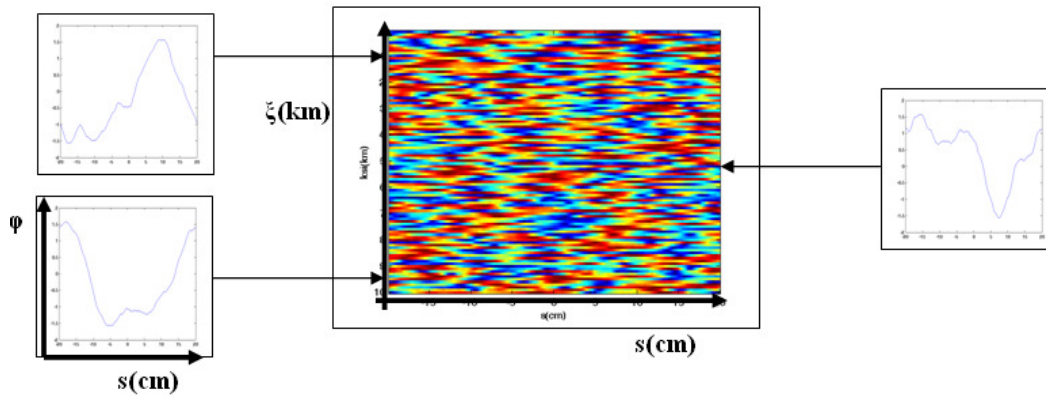Table 1: Correlation of Δn values to the optical potential *V* in our 1+1D

Figure 14: False color representation of a typical optical potential used in the s 1+1D simulations. The insets are the respective line profiles at various propagation distances. Higher values are denoted with red color and lower values with blue.

Some typical false colored intensity profiles of beams propagating in turbulence are shown in Figure 15. As the beam propagates from lower potential (785) to higher potential (1.57) its structure is different from the one in vacuum. The characteristics can recognized less in higher turbulence, than in lower. More specifically for $\Delta n = 5 \cdot 10^{-7}$, characteristics of the beams are almost invariant compared with vacuum, but for $\Delta n = 5 \cdot 10^{-5}$ characteristics cannot being recognized so easily.

Gaussian Beam	Airy Beam	2 Airy Beams that collapse

Atmospheric Turbulence for Δn=5·10⁻⁷

Atmospheric Turbulence for Δn=5·10⁻⁶

Atmospheric Turbulence for Δn=5·10⁻⁵
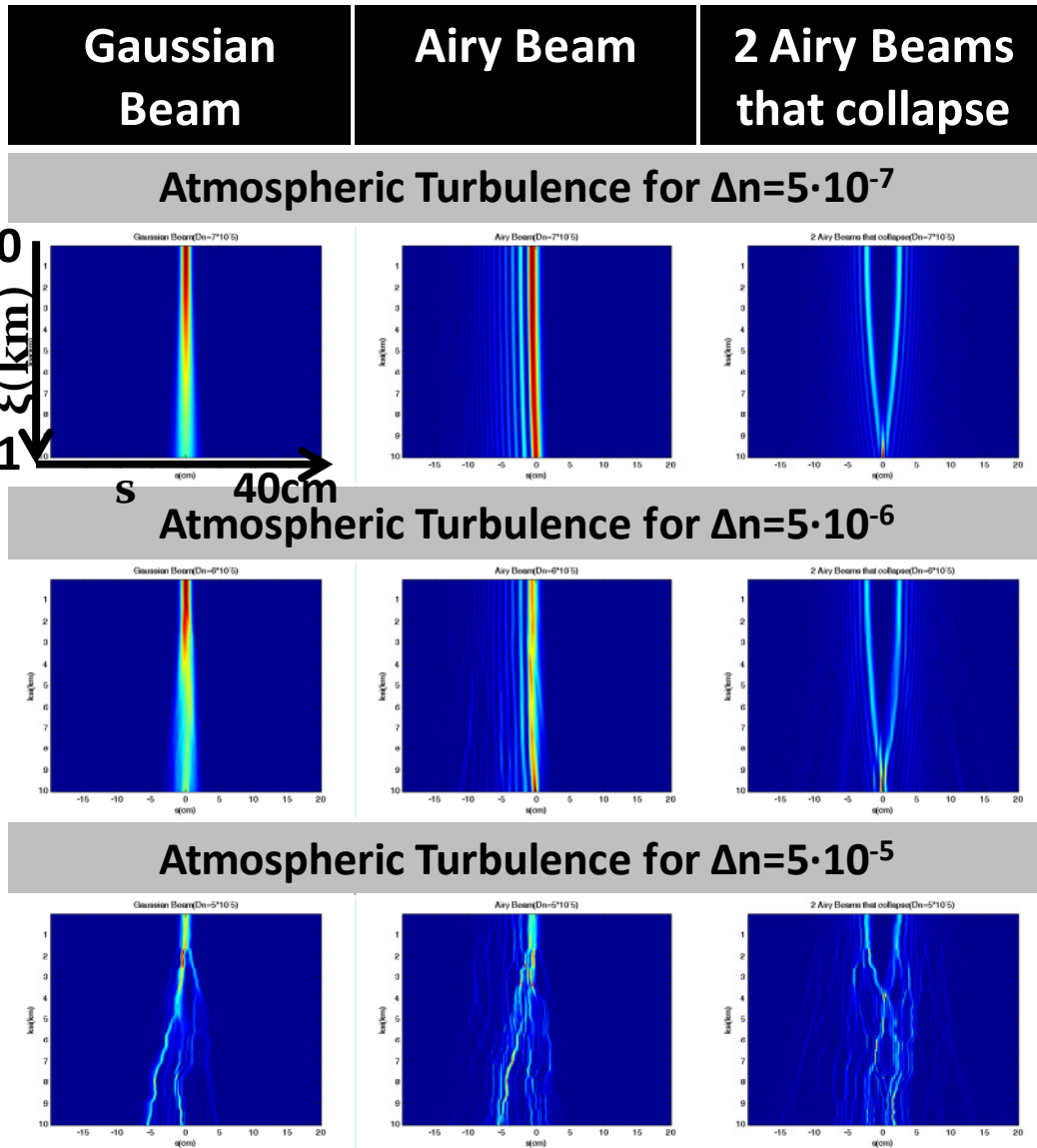
Figure 15: False colored intensity profiles for Gaussian, Airy and colliding Airy beams for various turbulence strengths (1+1D Beams propagation in atmospheric turbulence)

5.2 Scintillation Index

In order to characterize the irradiance fluctuations of a beam that propagates in a turbulent medium, scintillation index $(\sigma_I^{\,2})$ is used. It is given from the equation[22,23]:

$$\sigma_I^{\,2} = \frac{\left\langle I^2 \right\rangle - \left\langle I \right\rangle^2}{\left\langle I \right\rangle^2}$$

(58)

where I is the average intensity over an area of the beam and the angle brackets $\langle * \rangle$ denote averaging over the ensemble of turbulent media. The values of scintillation index represent the degree of coherence of the beam as it propagates through atmospheric turbulence. As the propagation distance is increased, scintillation index also increases, until it reaches the saturation level, where the scattering effect gradually weakens the focusing effect. The scattering affect is the reason that a beam loses its coherence. Lower values of scintillation index shows that beam coherence can be kept, a feature that is important in communications. The scintillation index is a quantitative measure of the signal variation due to turbulence on the detector in a typical communication link. Effectively turbulence can lead to a spreading and wobbling of the beam as a function of the time and this leads to a temporal variation of the signal strength in a finitely sized detector. Thus the scintillation index depends on the detector size (i.e. the area over which we average in eq. 58) and should decrease as the detector becomes large enough to collect the whole wobbling/scattered beam. Figure 16, shows the decrease in value of σ_I^2 as the diameter of the detector (area over which we average the intensity in eq. 58) increases (for $\Delta n = 10^{-6}$). It is clear that the effect is shadowed for detector sizes higher than. 0.1cm. Thus we choose to a receiver diameter of $2.1cm$, in our simulations. The number of realizations that is necessary for stabilization of the value of σ_I^2 is approximately 300, but in order our simulations of propagation to be more accurate 500 realizations were done for every different value of Δn (Figure 17). In Figure 17 are shown the scintillation index values for strong turbulence ($\Delta n = 5 \cdot 10^{-5}$) as a function of the number of realizations
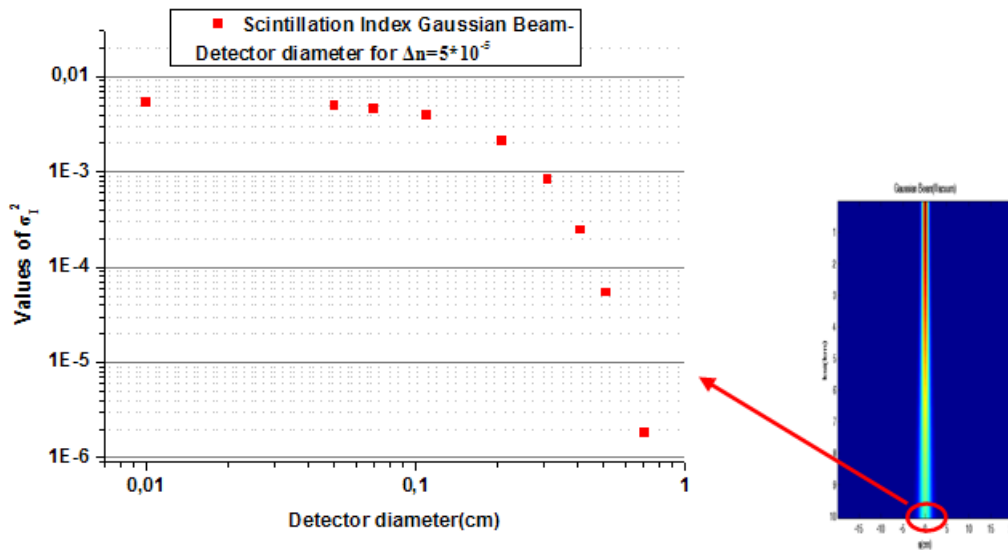
Figure 16: Scintillation Index as a function of the detector diameter. ($\Delta n = 5 \cdot 10^{-5}$ and number of realizations is 500)
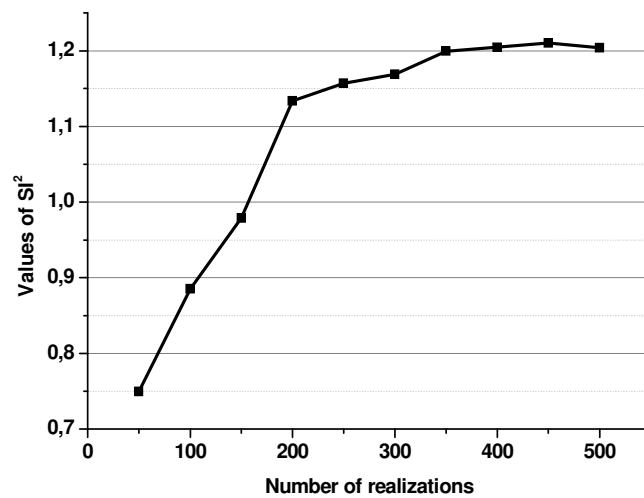

Figure 17: Scintillation Index as a function of the number of realizations

5.3 Results

To compare the effect of turbulence in different beam types we simulated the in 1+1D propagation, and calculated the respective scintillation index for the same media (optical potential). Figure 18 shows the scintillation index for 3 types of beams.
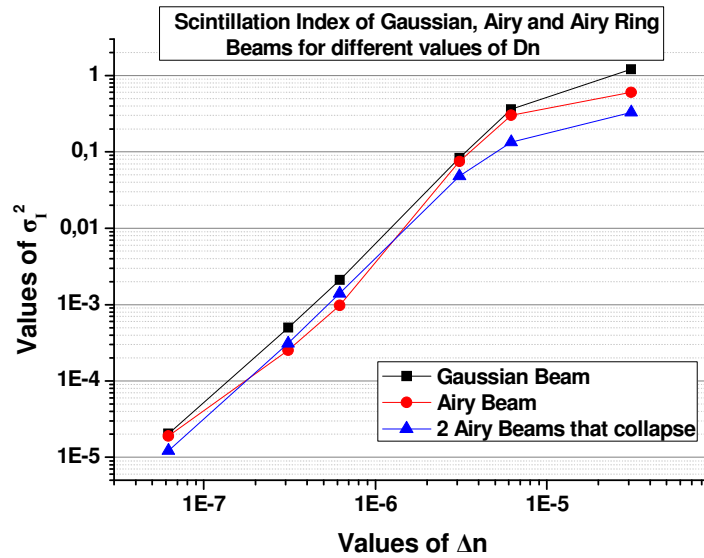
Figure 18: Comparative values of the scintillation index after propagation in 1 km of turbulent atmosphere.

In Fig. 18, it is shown that values of scintillation index for Gaussian beams are comparable, but bigger from Airy beams and from 2 Airy beams that collide. As turbulence is higher the colliding Airy Beams seem to be less affected by turbulence compared to the Gaussian beam. Airy beams exhibit a similar, but less efficient behavior. So from these first results one concludes that in optical link communication systems colliding Airy and Airy Beams should be better from Gaussian Beams in high turbulence. On the other hand, we should point out that for such strong turbulence all types of beams are severely deformed (Figure 15).

6.Numerical Modeling approach for 2+1D propagation

6.1 Phase screen model

The random spatio-temporal variation of the refractive index of atmospheric air leads to irradiance fluctuations in a propagating beam. In order to analyze these fluctuations in 2+1 dimensions, the method of random phase screens can be used. A random medium that extends between transmitter (source) and receiver (detector) can be well approximated by a system of thin phase screens that are equally placed along the propagation distance [References] (Figure 19).
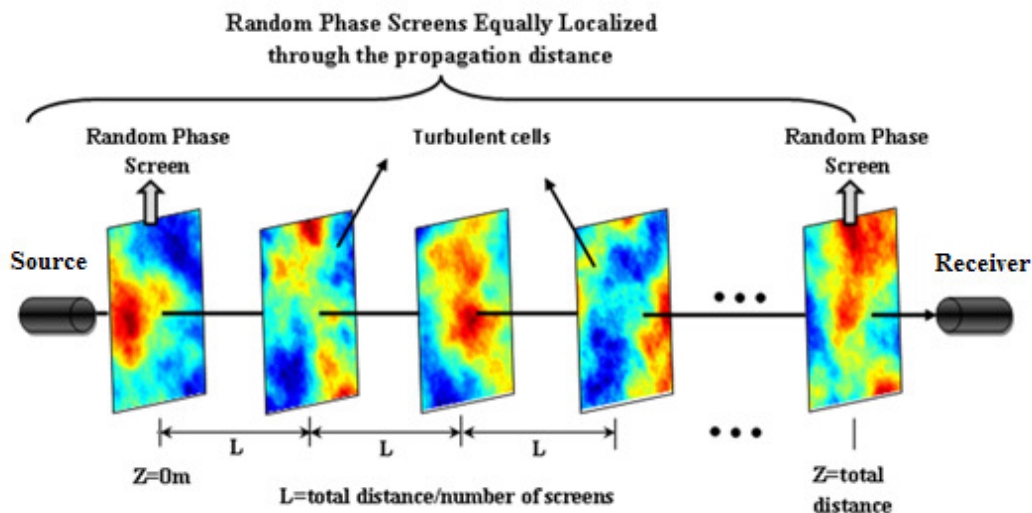
Figure 19: Schematic representation of the random phase screen model for propagation of two dimensional beams

In this thesis for the 2D propagation the random phase screen method initially proposed by Martin and Flatte is applied[24,25]. More specifically, the electric field of an optical wave that propagates along z direction is described by: $E(\mathbf{r},t)=f(x,y,z)\cdot e^{-i\cdot k\cdot z}$, where f is the wave amplitude, satisfying the parabolic approximation to the wave equation (Eq. 25):

$$2\cdot i\cdot k\frac{\partial f}{\partial z}+\overline{\nabla}_{\perp}^{2}f+V\cdot f=0 \tag{58}$$

where k is the wavenumber and V the optical potential. The split step solution of f at $z+\delta_{z}$ is given by:

$$f(x, y, z + \delta_z) = e^{i \cdot \phi(x,y,z)} \cdot \mathcal{F}^{-1} \left[f(z, K_\perp) \cdot e^{i \cdot K_\perp^2} \cdot \delta_z / (2 \cdot k) \right]$$

(59)

where $\mathcal{F}^{-1}$ is the 2D inverse Fourier transform in the perpendicular plane to the propagation direction (transverse plane), $f(z, K_\perp)$ is the Fourier transform of f at z, $K_\perp = \sqrt{\kappa_x^2 + \kappa_y^2}$ is the wavenumber in the transverse plane, and $\phi(x, y, z)$ is a function representing the accumulated spatial phase along the propagation from z to $z + \delta_z$.

The relationship between the phase $\phi(x, y, z)$ and the refractive index fluctuations of the medium is given by:

$$\phi(x, y, z) = \kappa \cdot \int\limits_{z}^{z+\delta_z} \Delta n(x, y, z) dz$$

(60)

The lack of complete knowledge of the spatial distribution of the refractive index along with the high computational cost renders the efficiency of this approach in simulations. The phase screen method bypasses this problem by using Markov's approximation to generate phase distributions $\phi(x, y, z)$, taking into account the power spectrum of the refractive index variations, at discrete positions along the propagation axis. According to this method a continuous random medium can be decomposed into a series of statistically independent phase screens, the 2D phase screen spectrum is given by:

$$\hat{\phi}(\kappa_x, \kappa_y) = 2 \cdot \pi \cdot \kappa^2 \cdot \delta_z \cdot \Phi_n(\kappa_x, \kappa_y, \kappa_z = 0)$$

(61)

It is based on the assumption that the correlation length of the irregularities in the medium is less than the separation between screens, but it permits to be characterized in the regime of weak fluctuations. This matter is important because these screens are statistically uncorrelated to each other so large separations δ_z can be used.

Each random phase screen is generated by properly filtering white Gaussian noise in order to obtain a random field with the desired second-order statistics. To implement this numerically a pseudo random complex numbers array $A + i \cdot B$ is firstly generated (appendix C). A and B are independent and random variation conforms to a particular probability distribution known as the normal distribution $\mathcal{N}(0,1)$ with mean value zero and standard deviation 1. The dimensions of this array are $N \times N$ (

N is the number of sampling points, in this thesis $N = 512$). This array is then multiplied by $\Delta_\kappa^{-1} \cdot \sqrt{\Phi_\theta(\kappa)}$, where $\Delta_\kappa^{-1} = 2 \cdot \pi \big/ N \cdot \Delta$ (Δ is the spatial sampling interval) and $\Phi_\theta(\kappa)$ is the phase power spectrum given by $\Phi_\theta(\kappa) = 2 \cdot \pi \cdot k^2 \cdot \delta_z \cdot \Phi_n(2 \cdot \pi \cdot \kappa)$, where Φ_n is the refractive index power density described by the von-Karman distribution (Eq. 51), k is the wavenumber ($k = \dfrac{2 \cdot \pi}{\lambda}$, with $\lambda = 0.8 \cdot 10^{-6} m$) and δ_z is the propagation distance between two consecutive screens and it is equal to the total propagation distance divided by the number of screens that are used for propagation ($\delta_z = Z/10 = 100 m$). According to the von Karman spectrum values of κ range from 0 to $1/L_0$. By inverse Fourier transforming the properly shaped random spectral phase distribution $(A + i \cdot B) \cdot \Delta_\kappa^{-1} \cdot \sqrt{\Phi_\theta(\kappa)}$ we retrieve the desired random phase field $\phi_1 + i \cdot \phi_2$. Since absorption effects are not taken into account in this thesis, only the real part is in the simulations. The parameters used in the estimation of the von Karman spectrum, are for the outer scale 5 m and for the inner scale 1 cm.
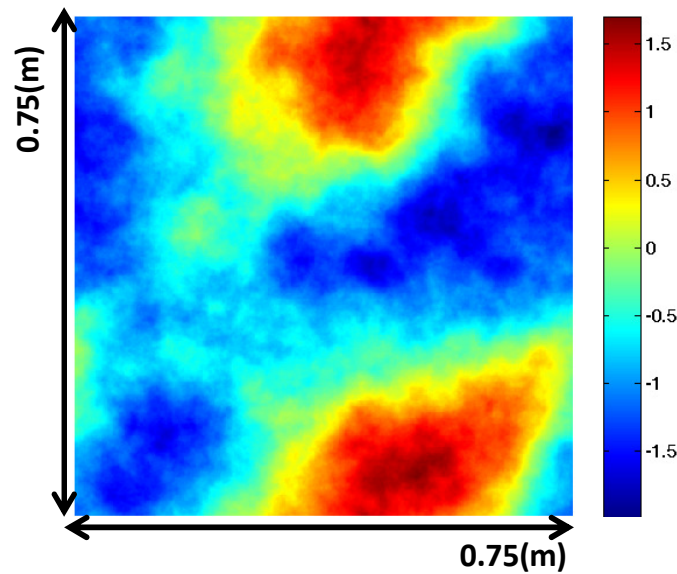

Figure 20: Typical example of a 512×512 synthesized random phase screen.

A typical example of a phase screen numerically synthesized using this approach way is shown in Figure 20. By using different values of inner and outer

scale, a variety of turbulence conditions can be simulated. As shown in Fig. 21 the scaling of the inner and out scale parameters has a profound effect on the simulated phase screens. The numerical algorithm used for the generation of the phase screens (in Matlab code) is shown in detail in Appendix C.
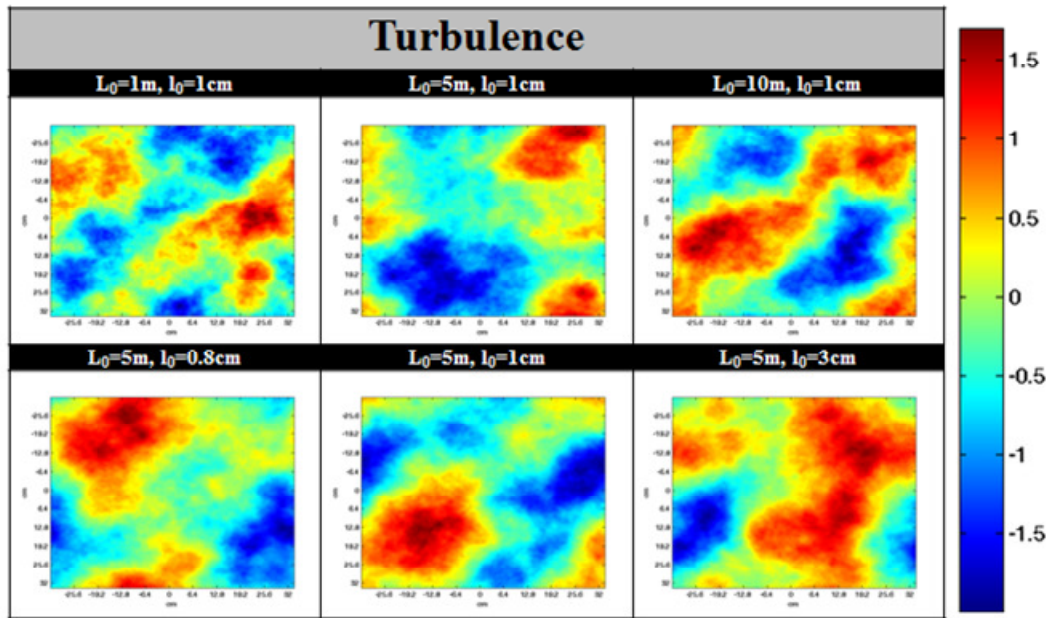

Figure 21: Typical phase screens (in false color) representing turbulence, for various values of the outer scale (L_o) and inner scale (l_o). The window size is 75cm×75cm

6.2 Simulation Method and parameters

The simulation of the propagation of optical beams in turbulent media is completed by combining the effect of turbulence, as described by the phase screens described in the previous section, with well know angular spectrum [26] propagation methods. The angular spectrum propagation method relies on the fact that the various spatial components of the Fourier spectrum of any complex field distribution can be identified as plane waves travelling in different directions away from the plane. The field amplitude at any other point (or across any other parallel plane) can be evaluated by adding the contributions of the plane waves, taking into account any phase shifts that took place during propagation. The Martin-Flatte model describes the propagation of an optical beam in a non-homogeneous medium as a two step process. The first step involves the effect of medium disorder, as a phase distribution added to

the phase of the initial beam, while the second step involves the propagation of this perturbed beam using the angular spectrum method. In this way the beam is numerically propagated from plane z to $z+\delta_z$. This process is iteratively repeated from one plane to the other until the desired propagation distance. Since no solution of a PDA is involved the method is not computationally intense and is well suited for propagation along large distances.
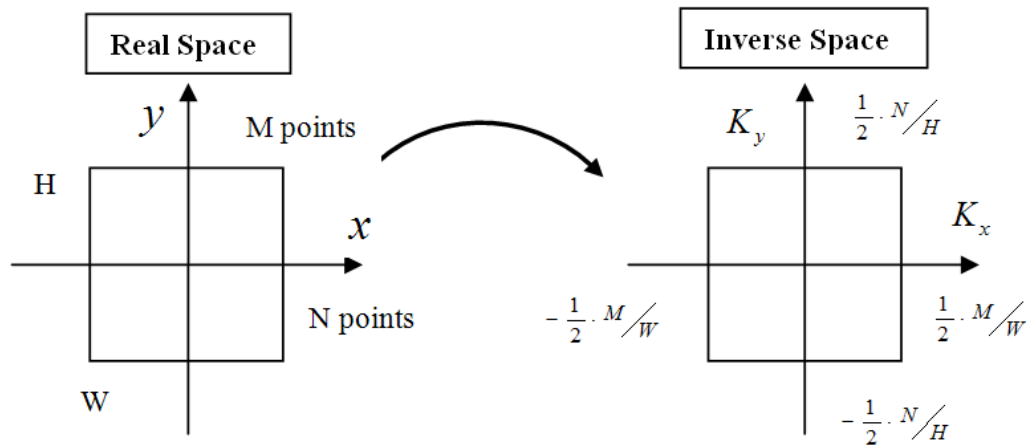

Figure 22: Discretization of the problem in the real (x, y) and the inverse (K$_x$, K$_y$) space. For window size W×Z (N×M points) in real space, the corresponding inverse space dimensions are $\frac{M}{W} \times \frac{N}{H}$ (K$_x$× K$_y$)

The discretization of the propagation problem in the real (x, y) and the inverse spatial frequency space (Kx, Ky) is depicted in Fig 22. The physical width W and the height H of the simulation window are related to the lowest spatial frequency that can be resolved $K_x^{\min} = 1/W$ and $K_y^{\min} = 1/H$ respectively. On the other hand the highest spatial frequency is also correlated to the number of sampling points so $K_x^{\max} = M/W$ and $K_y^{\max} = N/H$.

In all our simulations the transverse coordinates (x, y) are discretized to 512x512 sampling points while 10 steps, and thus 10 phase screens, are used for the propagation along z direction. The wavelength used is $\lambda = 0.8 \cdot 10^{-6} m$ and the wavenumber is $k = \frac{2 \cdot \pi}{\lambda}$. The physical size of our simulation window is $0.75 \times 0.75 m$, while the total propagation distance is 1 km thus the inter-screen distance is 100m. In our simulations we studied the propagation of Gaussian, Airy, Bessel and Airy Ring beams (eq. 26) under the action of weak and strong turbulence .

The simulated beam parameters are: the Gaussian beam waist is $w_0 = 5cm$, Airy Beam width is $w_x = w_y = w_0 = 5cm$ and $a = 0.05$, Bessel beam width is $w = 5cm$ and for the Airy Ring Beams the radius $r_0 = 5cm$ and the corresponding constants are $w = 4.85 \cdot 10^{-3}$ and $a = 0.05$.

The initial beam, after proper manipulation of required values of parameters, is spatially Fourier transformed. The effect of propagation of each plane wave component of the angular spectrum is evaluated by a multiplication by the paraxial transfer function:

$$T = \exp\left(-\frac{i \cdot \lambda}{4 \cdot \pi} \cdot \delta_z \cdot \left(\kappa_x^{\;2} + \kappa_y^{\;2} \right) \right) \tag{62}$$

where κ_x, κ_y are the transverse spatial frequency components and δz denotes the propagation distance. The new field is the evaluated by inverse Fourier transforming in space domain.

The 2D+1 propagation algorithm (in Matlab code) used in our simulations is described in detail in appendix D. The results of numerical simulation of the propagation of various beams in homogeneous atmosphere ($\Delta n = 0$) is represented in Figure 23. Gaussian, Airy and Bessel Beams stay almost unalterable at the simulated propagation distances, whereas Airy Ring Beams focus in ~1km.

Gaussian Beam	Airy Beam	Bessel Beam	Airy Ring Beam

Propagation Distance=100m

Propagation Distance=400m

Propagation Distance=700m
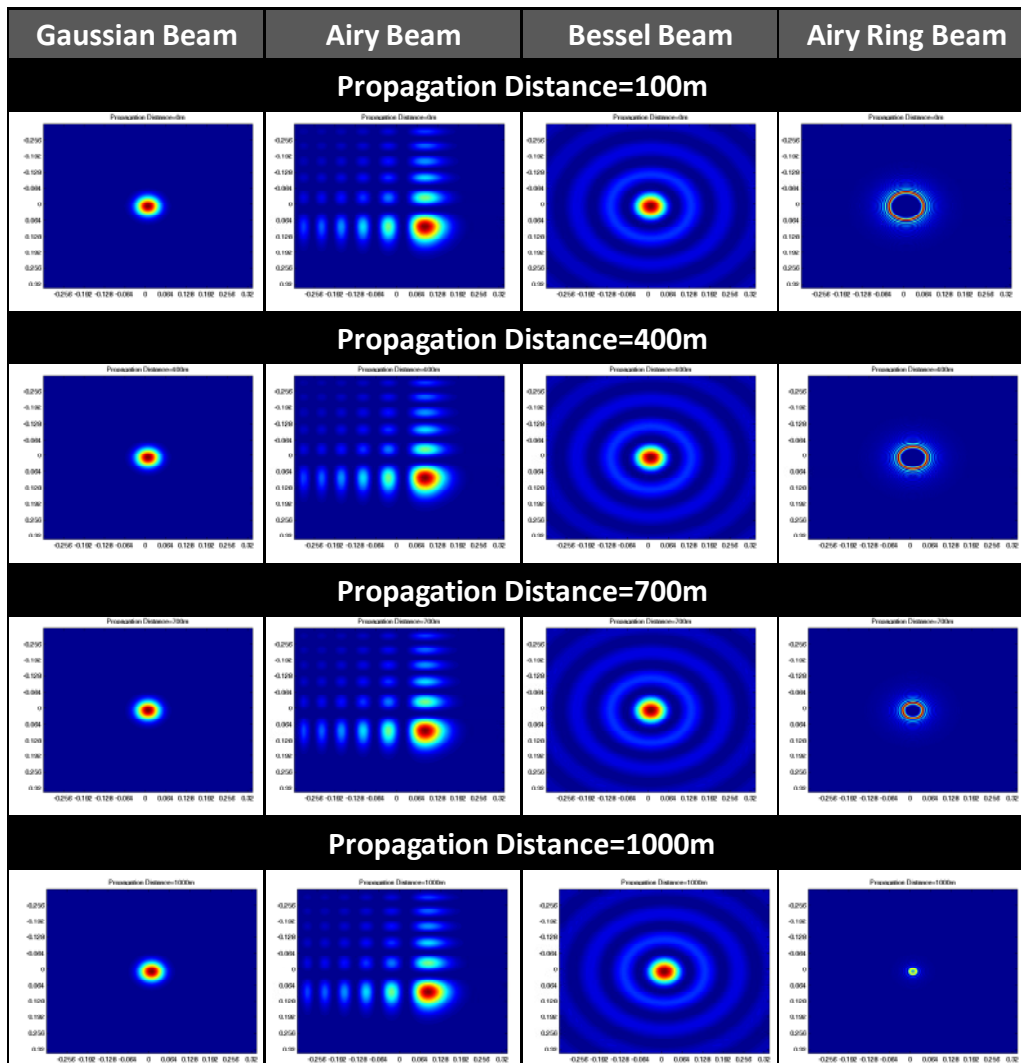

Propagation Distance=1000m

Figure 23: Simulated intensity profiles (normalized) as a function of the propagation distance in homogeneous atmosphere ($\Delta n = 0$) for various beam types. The window size is 75cm×75cm.

In order to check the numerical accuracy of the propagation algorithm we compared the simulation results with the analytical solution of the propagation of a a Gaussian Beam. The normalized intensity, retrieved from analytic calculations and the numerical simulation, for a Gaussian beam with waist $w_0 = 7mm$ is shown in Fig. 24 for a propagation distance of $2km$. The small discrepancy between the simulation results and the analytic solution is well below 1.5 % in all cases is related to the discretization points (N=512) and can reduced as this number is increased. On the other hand the attained accuracy is adequate for the specific application.
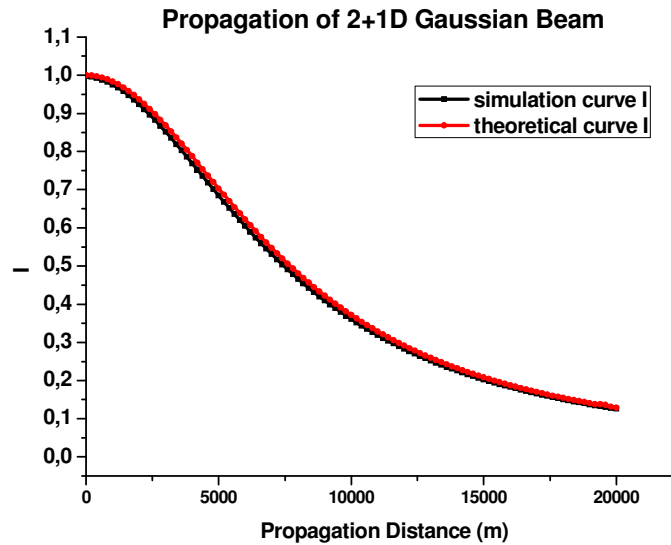
Propagation of 2+1D Gaussian Beam

Figure 24: Comparison of numerical results retrieved using the propagation code, to analytic prediction for a Gaussian beam with waist w0=7cm.

In the study of propagation of non-diffracting beams in turbulent media one cannot ignore the simple plane wave. Plane waves a trivial non-diffracting, infinite energy, solution of the wave propagation equation. They simplicity makes them a very good reference for the propagation of more complex waves such as the Airy beams. The propagation of plane waves in turbulent media has been extensively studied [References 12, 13, 14, 18, 19, 21, 22, 24] mainly in the field of astronomy.

We preformed simulations for plane waves propagating in turbulent media using the phase screen model. Figure 25 depicts typical results of intensity profiles of plane waves after 1 km of propagation through various strengths of turbulence. The parameters used in the simulations are L_o= 5 m, l_o= 1 cm, W=H=75cm. For weak turbulence $C_n^2 = 10^{-18}$ hot spots in the form of speckles start to form, but in general their maximum intensity varies only by 5%. For stronger turbulence and $C_n^2 = 10^{-17}$, the speckles start to coalesce forming hot spots that stand out from the background. For even stronger turbulence ($C_n^2 = 10^{-16}$) the speckle size has dramatically decreased, while the speckle density has increased leading to a typical scattering signature with some large scale average intensity variations, indicative of a dissipative regime. This behavior is further enhanced for very strong turbulence ($C_n^2 = 10^{-15}$) where the scattering is so strong that the average intensity is spatial homogeneous and

the signal has dramatically dropped since energy is strongly dissipated by small scale refractive index variations (smaller than l_o).
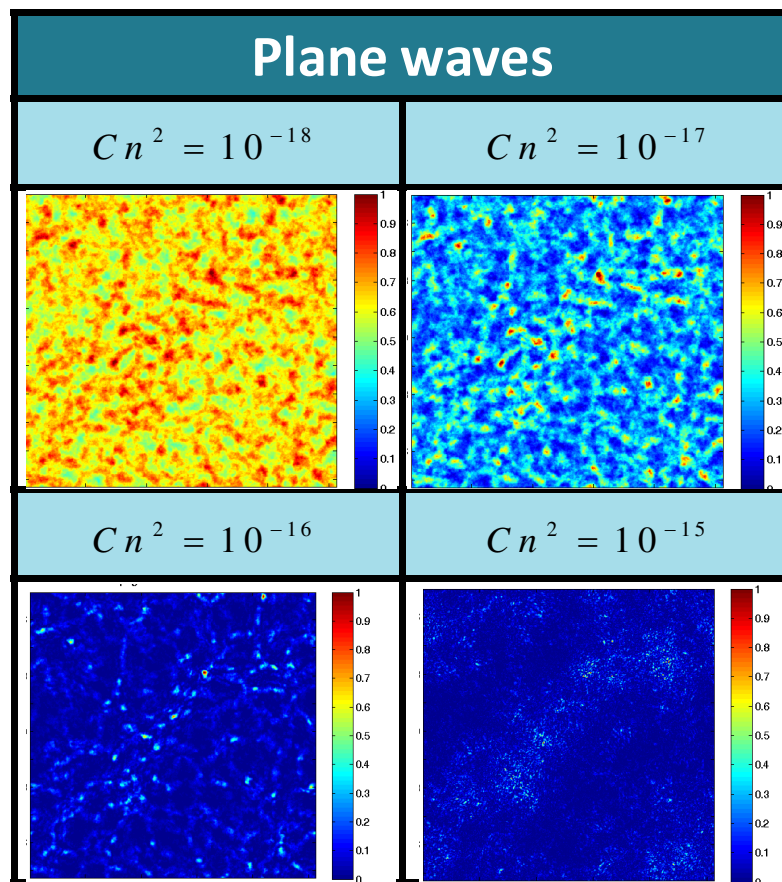

Figure 25: Typical simulated intensity profiles (in false color) after propagation of plane waves in turbulent air (propagation distance =1 km, L_o = 5m, l_o=1cm, window size is 75cm×75cm)

The next step is to study the propagation of Gaussian Beams in turbulent media. Gaussian beams are not non-diffracting but they stand as a good reference to compare with the non-diffracting beams (Airy and Bessel) we are interested in as well as with the also "diffracting" Airy Ring Beams. Figure 26 depicts comparative simulation results after 1 km of propagation of all the above mentioned types of beams in the same turbulent media as a function of the turbulence strength. Plane wave propagation is also depicted here to help identify the different propagation regimes. The propagation distance of 1 km is well within the Rayleigh zone of the Gaussian Beam used as typical for an optical communication link. Furthermore, the primary lobe sizes for the Airy and Bessel beams, and the primary radius of the Airy Ring beam, are set equal to the FWHM of the Gaussian beam. Finally, the focus of the Airy Ring beam is set, by tuning the width of the primary lobe, to 5cm.

As it is shown in Fig. 26 at low turbulence values ($C_n^2 = 10^{-18}$) the Gaussian beams are weakly affected. At moderate turbulence ($C_n^2 = 10^{-17}$) the Gaussian Beam profile starts to degrade while for strong and very strong turbulence ($C_n^2 \geq 10^{-16}$) the beam profile is severely damaged with speckles, hot spots, and finally with strong scattering indicative of a strongly dissipative regime.
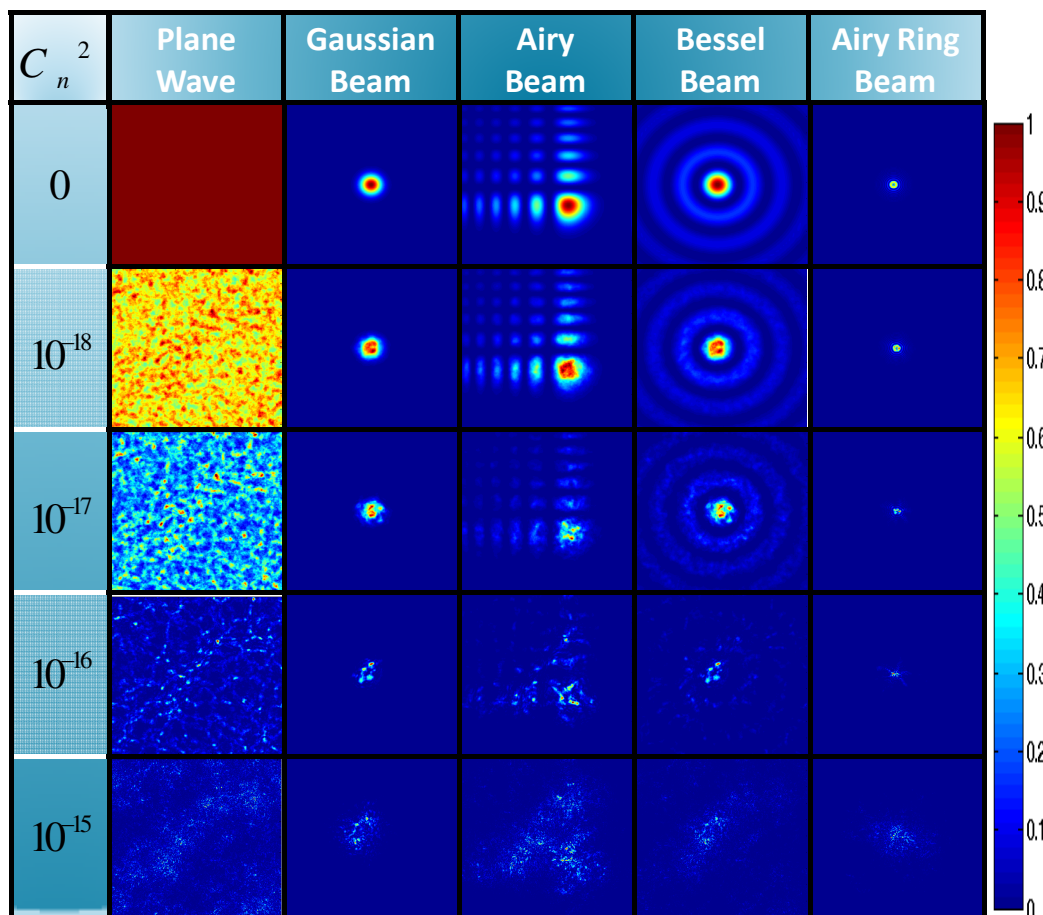

Figure 26: Simulated intensity profiles as a function of the turbulence strength (C_n^2) for various beams after propagation in 1 km of turbulent atmosphere. (window size is 75cm×75cm).

In the case of Airy Beams, as shown in Fig, 26 low turbulence ($C_n^2 = 10^{-18}$) has a minor effect on the intensity distribution, mainly of the primary lobe. At moderate turbulence for ($C_n^2 = 10^{-17}$) hot spots and speckles start to form on the intensity lobes while the lobe structure remains unaffected. For strong and very strong turbulence ($C_n^2 \geq 10^{-16}$) we enter the scattering and energy dissipation regime. The lobe structure is practically lost while some hints of the beam symmetry still remain.

Bessel Beams exhibit a similar behavior. In low turbulence ($C_n^2 = 10^{-18}$) the intensity distribution is weakly affected mainly in the primary lobe accompanied with some speckling in the rings. For moderate turbulence ($C_n^2 = 10^{-17}$) hot spots start to form on the primary lobe while speckles are clearly visible on the rings. As in the Airy beams the lobe structure remains unaffected. In strong and very strong turbulence ($C_n^2 \geq 10^{-16}$) scattering and energy dissipation are profound. The lobe structure, as in the Airy beams, is also lost while only hints of the beam symmetry still remain.

Finally, as shown in Fig, 26 Airy Ring Beams exhibit and interesting behavior. We have although to keep in mind that in contrast to the previous beams they are not non-diffracting, although the exhibit some "self-healing" capability. Furthermore, they are self-focused very close to the observation plane so energy is concentrated in a very small area. As with the rest of the beams we hardy observe any effect in the beam profile when turbulence is low ($C_n^2 = 10^{-18}$). At moderate and strong turbulence ($10^{-17} \leq C_n^2 \leq 10^{-16}$) the focus is still preserved with some peripheral ray structured scattering. Finally for very strong turbulence ($C_n^2 = 10^{-15}$) we enter the scattering and energy dissipation regime with complete loss of the beam structure. We have to note though that energy is spread to an area similar to that of the Gaussian beam.

Summarizing these results we can distinguish three regimes the weak, moderate and strong turbulence. For all beams the weak turbulence ($C_n^2 < 10^{-17}$) had minor effect in the intensity profiles. In the case of moderate turbulence ($10^{-17} < C_n^2 < 10^{-16}$) hot spots and speckles started to appear, affecting the beam profile, in all beams except the Airy ring beams. For strong turbulence ($C_n^2 \geq 10^{-16}$), severe scattering leads to energy dissipation in all beams with the Airy ring distribution exhibiting the weakest deteriorating effect..

6.3 Scintillation Index

As was mentioned in section 5.3 Scintillation Index that characterizes intensity fluctuations is given by the equation[27]:

$$\sigma_I^2 = \frac{\langle I^2 \rangle - \langle I \rangle^2}{\langle I \rangle^2} \qquad (63)$$

where I is the irradiance of the beam and the angle brackets $\langle * \rangle$ denotes the average. In the bibliography this average can be calculated using two different approaches which are be analyzed in detail in Appendix E.

Using the results of Fig, 37 (Appendix E) we choose a detector of $0.45cm$. In Fig. 27 the scintillation index as a function of the number of independent realizations is shown. The minimum number of realizations that is necessary for the stabilization of the σ_I^2 value is ~50, in contrast to the 1+1D model, where 300 realizations were needed. Taking into account these results, we used at least 150 realizations in all our propagation simulations.
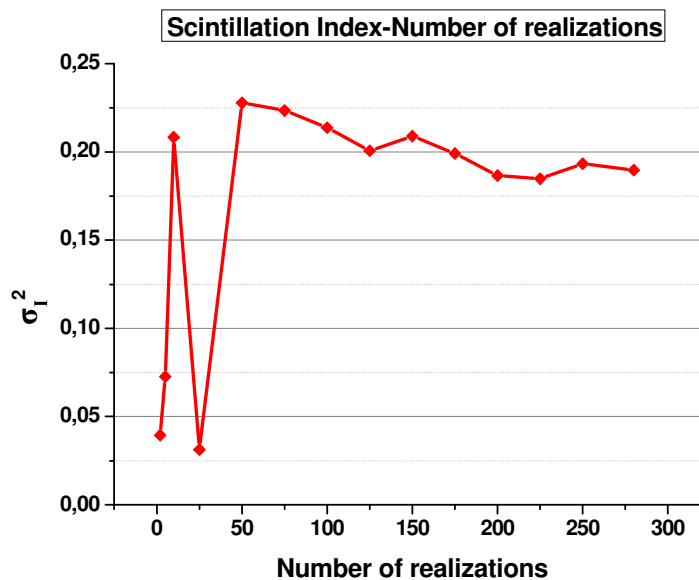
Figure 27: Scintillation index (σ_I^2) as a function of the number of simulated realizations ($C_n^2 = 10^{-18}$)

6.4 Results

The scintillation index is proper single valued quantitative measure of the effect of turbulence in a communication link. Fig. 28 depicts comparative results of the scintillation index σ_I^2 as a function of the propagation distance for Gaussian, Airy and Bessel beams and for various amounts of turbulence.
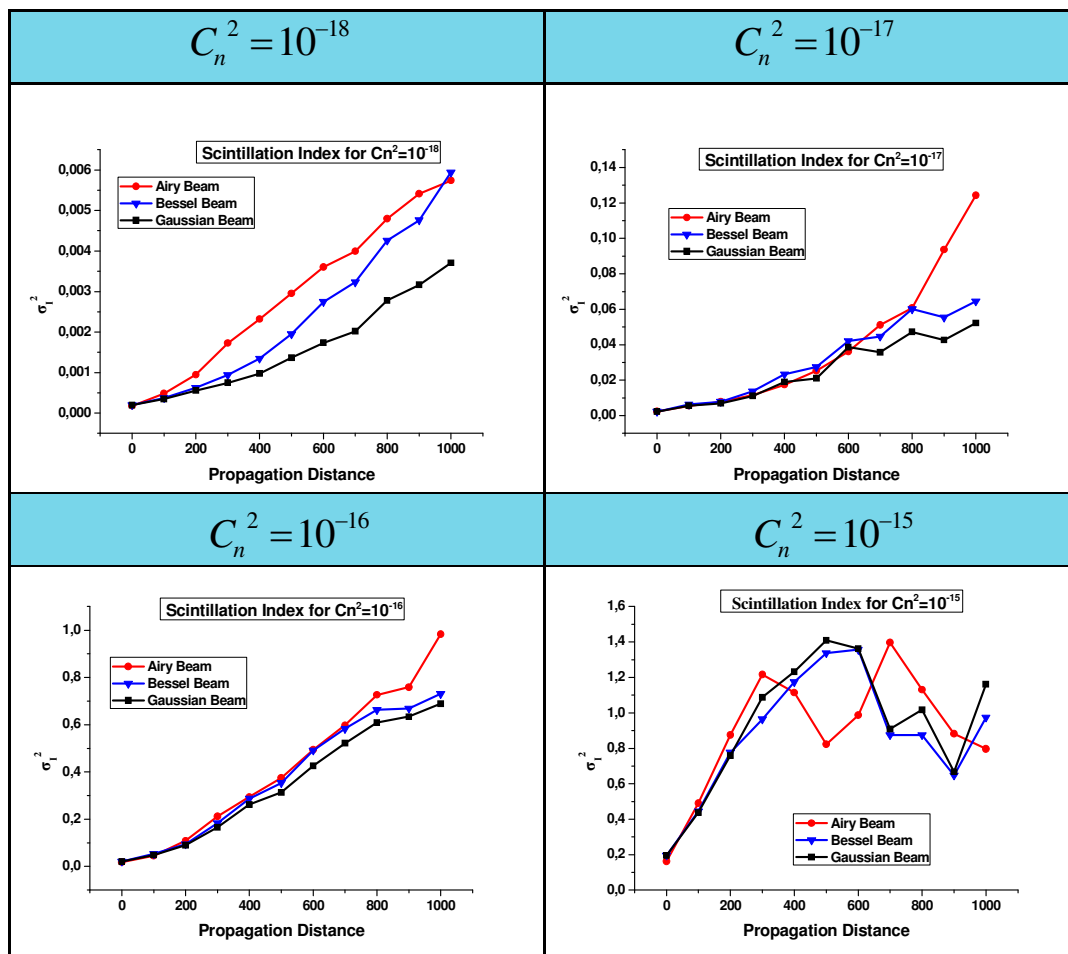

Figure 28: Scintillation index (σ_I^2) as a function of the propagation distance. The simulations are preformed for Gaussian, Airy and Bessel Beams for varying turbulence strength (C_n^2)

At low turbulence ($C_n^2 = 10^{-18}$), Gaussian Beams exhibit minimal scintillation. The difference between Bessel Beams and Airy Beams starts after $300m$ of propagation, until then they have almost the same values. The next higher turbulence is for $C_n^2 = 10^{-17}$. It is observed that Gaussian and Bessel Beams have the same response and their values of σ_I^2 are proportional, with values of Gaussian Beams

being smaller. Their values start to have bigger difference after $600m$ of propagation in the medium. Airy Beams at this turbulence response different from the other beams. Until $600m$ of propagation, they have the same behavior (or a little better) as Gaussian Beams, but after this distance their values start to size compared to the other beams.

In row comes higher turbulence, for values of $C_n^{\,2} = 10^{-16}$, the values of $\sigma_I^{\,2}$ are almost same and beams seem to have the same response to the turbulence. Gaussian Beams are a little better and Airy Beams are a little worse. The beams haven't collapsed for this turbulence and values of $\sigma_I^{\,2}$ over propagation distance increase at each step of propagation. The last medium of propagation and with the highest turbulence is given for $C_n^{\,2} = 10^{-15}$. Gaussian and Bessel Beams' values of $\sigma_I^{\,2}$ have the same response to this medium, but Bessel Beams have lower values. Their $\sigma_I^{\,2}$ values until $500m$ increase, they have peak value at this propagation distance and after that they start to decrease. However, Airy Beams have a different response to the medium and their value of $\sigma_I^{\,2}$ at $1km$ propagation distance is lower compared to the other types. All beams seem to crush for this medium and this explains the peak value of $\sigma_I^{\,2}$.
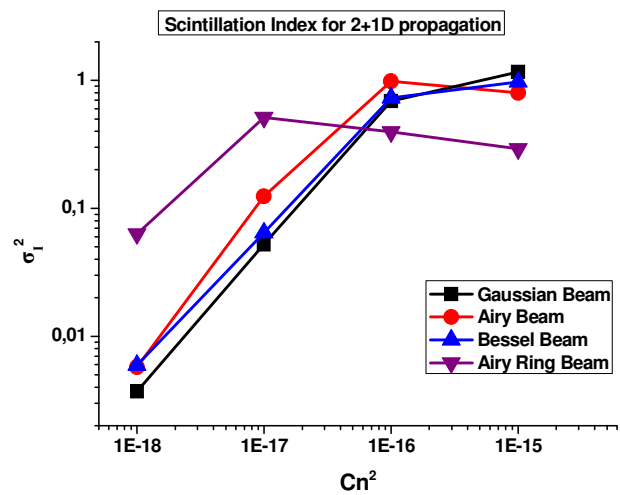

Figure 29 Scintillation index (σ_I^2) as a function of the turbulence strength (C_n^2). The (2D +1) simulations are preformed for various beams.

In Fig. 29, are shown the comparative results of the scintillation index $\sigma_I^{\,2}$, as a function of the turbulence strength, for the propagation though 1 *km* of turbulent atmosphere for Gaussian, Airy, Bessel and Airy Ring beams. The behavior is not

monotonic and strongly depends on the beam type. Interestingly, at higher values of turbulence ($C_n^2 > 10^{-16}$) Airy Ring Beams exhibit considerably lower scintillation, compared to the Gaussian, Airy and Bessel beams.

At following graphs (Fig. 30, 31) we present the way that beams propagate for longer distance. The propagation was done for 10km and the number of screens used was 20 screens. These simulations were preformed to test the self healing properties of non-diffracting beams. Only propagation at low ($C_n^2 = 10^{-18}$) and moderate ($C_n^2 = 10^{-17}$) turbulence were studied since for strong and very strong turbulence ($C_n^2 > 10^{-16}$) scattering and energy dissipation take place already from 1 km in all beam types (Fig. 26). At first for low turbulence ($C_n^2 = 10^{-18}$) Gaussian Beams even from 3km start to focus and after this distance they scatter and deform. Airy Beams seem to have same effect on their intensity distribution, mainly on the primary lobe for propagation until 3km, but on the other intensity lobes, apart from main lobe, hot spots and speckles start to form on. Bessel Beams exhibit a similar behavior until 3km, but for larger distance they deform and speckles are clearly visible on the rings. In moderate turbulence ($C_n^2 = 10^{-17}$) all beams at 3km are almost unrecognizable, hot spots start to form. In order to compare them for communications links their scintillation index will be examined.
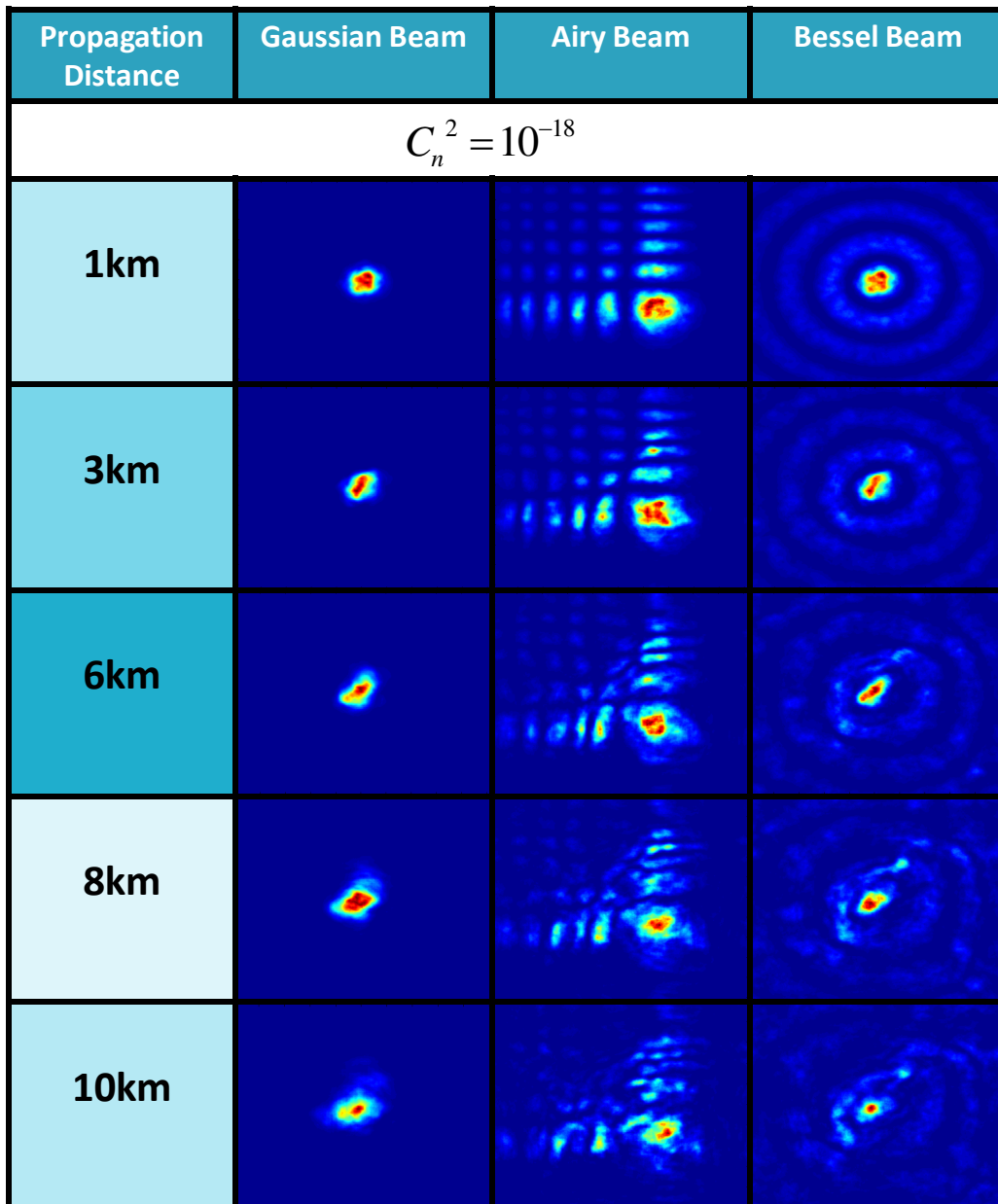
Propagation Distance	Gaussian Beam	Airy Beam	Bessel Beam
$C_n^2 = 10^{-18}$			
1km			
3km			
6km			
8km			
10km			

Figure 30: Propagation of Gaussian and non-diffracting beams for propagation distance 10km, turbulence strength $C_n^2 = 10^{-18}$ and window size 75cm×75cm.
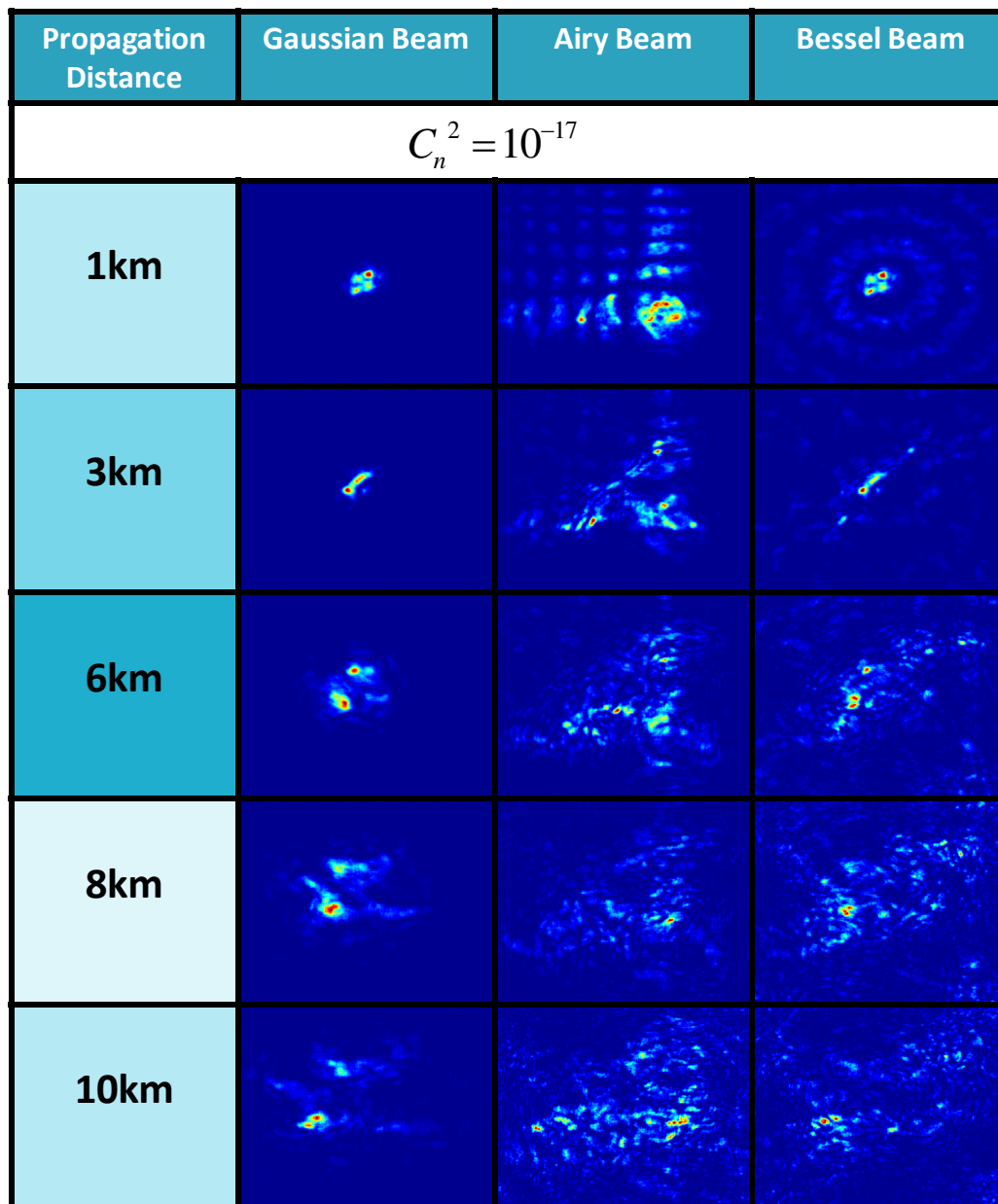
Propagation Distance	Gaussian Beam	Airy Beam	Bessel Beam
$C_n^2 = 10^{-17}$			
1km			
3km			
6km			
8km			
10km			

Figure 31: Propagation of Gaussian and non-diffracting beams for propagation distance 10km, turbulence strength $C_n^2=10^{-17}$ and window size 75cm×75cm.

Fig. 32 depicts the scintillation index as a function of the propagation distance, for low and moderate turbulence. Interestingly, for low turbulence Airy beams between for 4 and 7km exhibit slightly lower scintillation compared to Gaussian and Bessel beams possibly due to their self healing properties. Even for moderate turbulence they seem to have better response. Although, in this case the values of σ_I^2 so we are already in a regime that is improbable for a communication link.
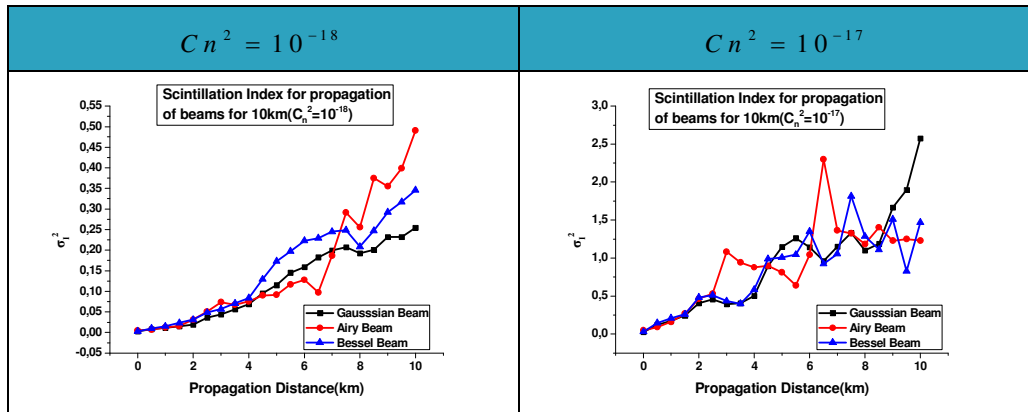
Figure 32: Scintillation index of Gaussian Beams and non-diffracting Beams for low ($C_n{}^2=10^{-18}$) and moderate ($C_n{}^2=10^{-17}$) turbulence for propagation distance 10km. Detector diameter used was 0.45cm.

6.5 The effect of beam size

In previous simulations the primary lobe width of the Airy Beams was chosen be equal to the FWHM of the Gaussian beam. This lead to an Airy beam with total extent which was considerably larger than the extent of the reference Gaussian beam and can lead to biased results in the case of turbulent media. In order to study the effect of beam size in the propagation through turbulent media we preformed numerical simulations for Airy beams with different widths (w_o= 0.63, 1.25 and 5 cm) keeping all the rest simulation parameters the same as at previous 2+1D simulations. Figure 33 depicts our simulation results after propagation though 1 *km* of turbulent atmosphere as a function for various turbulence strengths. It is clear that as the beam size gets smaller the deteriorating effect of turbulence weakens. Even for strong turbulence ($C_n^2 = 10^{-16}$) the smallest Airy Beams (w_o= 0.63 *cm*) still maintain their primary lobe although severe scattering is also present. The same behavior is exhibited by intermediately sized Airy Beams (w_o= 1.25 *cm*) which also preserve, although not that efficiently, their primary intensity lobe. For very strong turbulence ($C_n^2 \geq 10^{-15}$) strong scattering takes place and energy dissipation and beam diffusion are prominent for all cases.
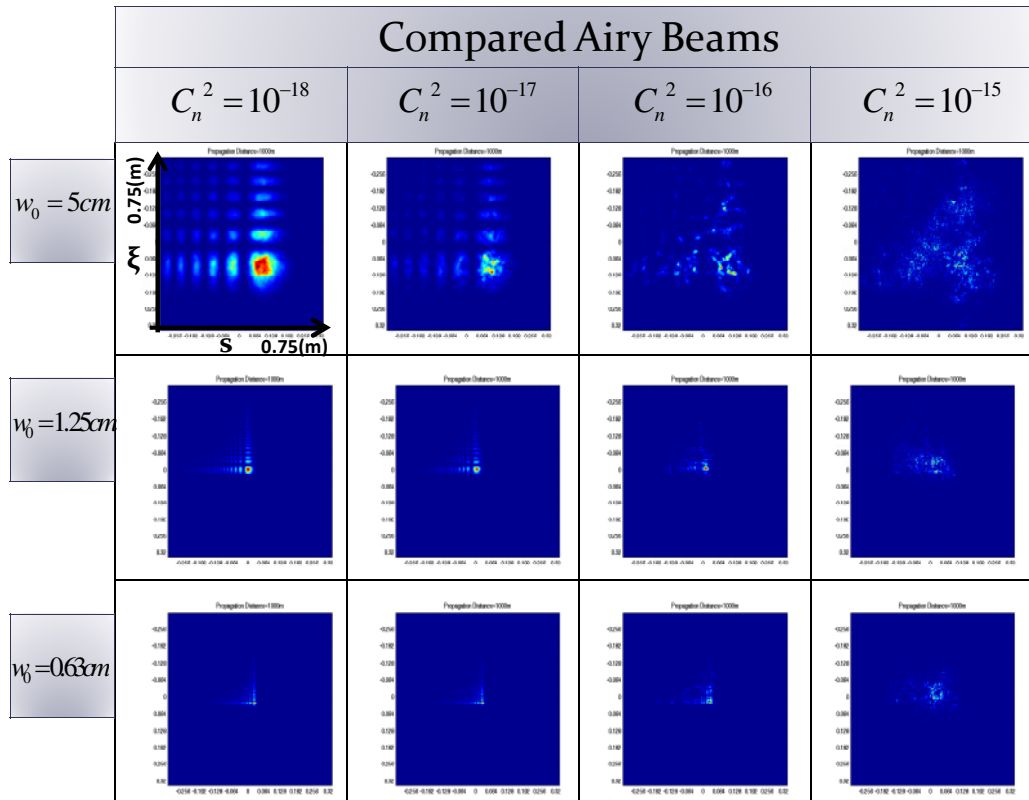
Compared Airy Beams			
$C_n^2 = 10^{-18}$	$C_n^2 = 10^{-17}$	$C_n^2 = 10^{-16}$	$C_n^2 = 10^{-15}$

Figure 33: Simulated intensity profiles as a function of the turbulence strength (C_n^2) for differently sized Airy beams after propagation in 1 km of turbulent atmosphere

Fig. 34 depicts the respective scintillation index σ_I^2 for all the simulated Airy beams in comparison to the reference Gaussian beam. The diameter of the detector for computing σ_I^2 is again 0.45 *cm*. It is evident that the size of a beam has a dramatic effect on the scintillation values. In all cases the smallest Airy beams exhibit the lowest σ_I^2 values. The scintillation index depends in a non-monotonic fashion to the turbulence strength in all cases. For very strong turbulence the σ_I^2 values tend to stabilize around $\sigma_I^2 \sim 1$.
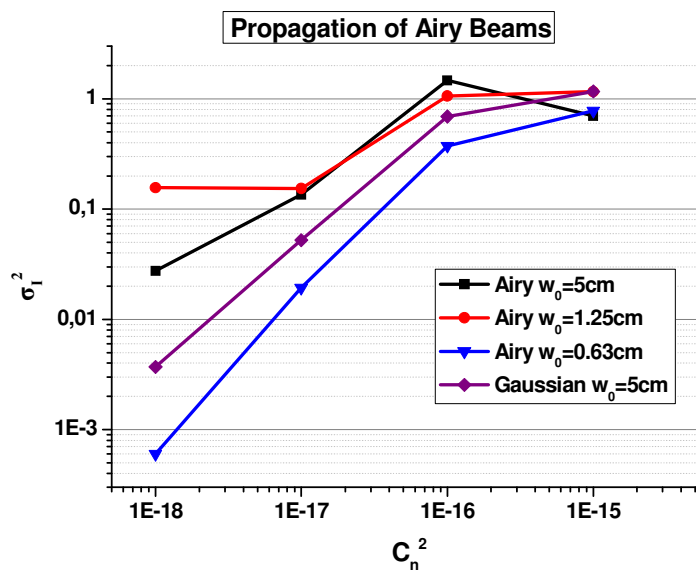
Figure 34: Scintillation index (σ_I^2) as a function of the turbulence strength (C_n^2) for Airy Beams (with different values of w_0) simulated for 2+1D propagation and compared with Gaussian Beam (w_0=5cm)

6.6 Model for 1+1D propagation through phase screen model

Until now, two methods for the numerical simulation of the propagation of optical beams in turbulent media beams were presented. The first one was the direct numerical solution of the paraxial propagation PDE for 1+1D and the second one was use of a split step approach utilizing phase screens and the angular spectrum model (Martin-Flatte model) for 2+1D propagation. To directly compare the efficiency of each model in the same regime we also preformed 1+1D propagation simulations using Martin-Flatte model.

In this case we simulated 1D Gaussian and Airy Beams, with width (primary lobe for the Airy) w= 5 cm. The beams were numerically propagated though 1 km of turbulent atmosphere and the physical window size was set to 0.75 m as in the previous simulations. Fig. 35 depicts intensity profiles of the propagated beams for different values of turbulence (C_n^2). It is shown that for lower values of C_n^2, which correspond to low turbulence Gaussian Beams are more coherent, whereas for high turbulence ($C_n^2 > 10^{-16}$) Airy Beams are more coherent.
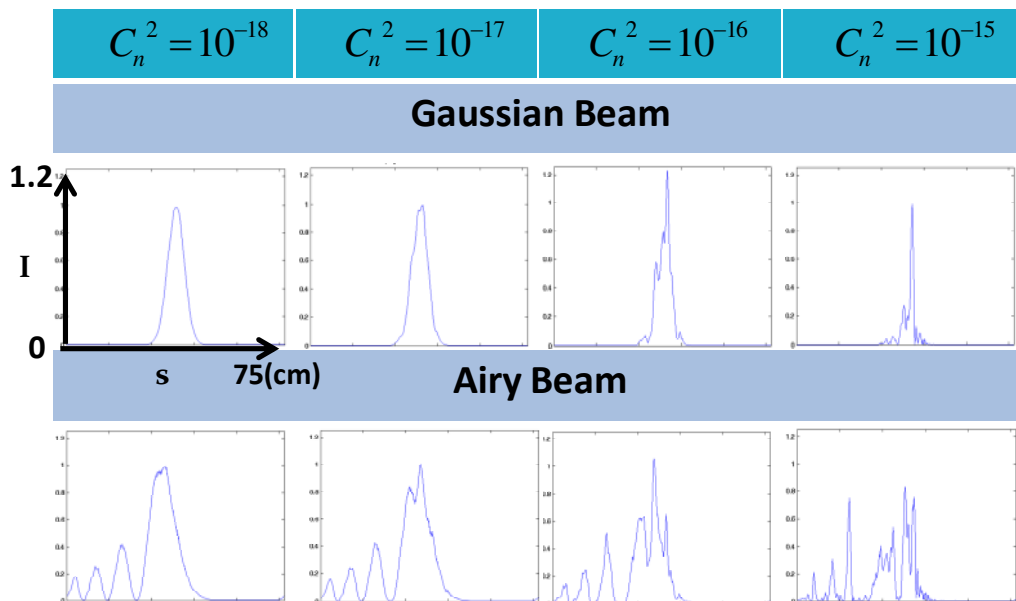
Figure 35: 1+1D simulated intensity profiles using phase screen model as a function of the turbulence strength (C_n^2) for Gaussian and Airy Beams after propagation in 1 km of turbulent atmosphere.

The same results also came from computation of σ_I^2 for the compared beams. As it is shown in Figure 36, values of scintillation index of the beams are close to each other. As turbulence gets higher values, Airy Beams have better response.
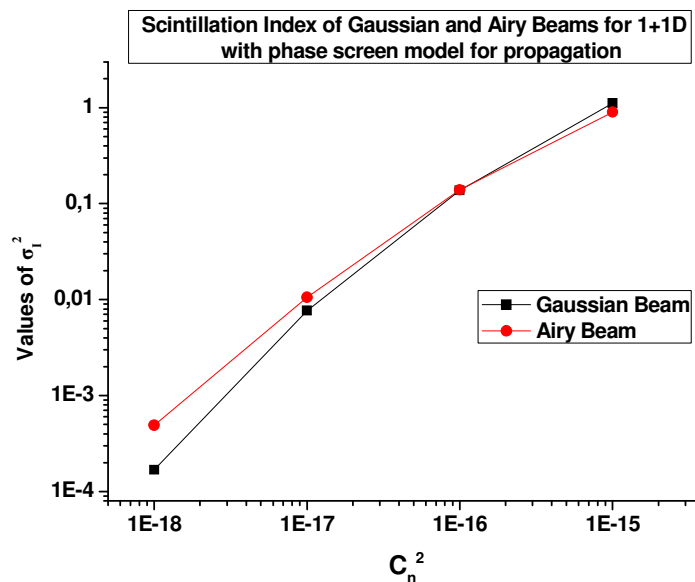

Figure 36: Scintillation index for 1+1D propagation of Gaussian and Airy Beams with phase screen method

7 Conclusions and Discussions

As a conclusion, our simulations show that in general turbulence can have a serious deteriorating action in non diffracting beams. The self healing action is obviously not enough to overcome turbulence. By continuously scrambling the wavefront along their propagation turbulence effectively cancels the continuous energy flow from peripheral structures to their primary intensity lobe and thus eliminates the self healing.

On the other hand, by properly tuning their size Airy beams can be tuned to withstand turbulence quite better that the commonly used Gaussian Beams. Interestingly, Bessel Beams, most probably due to their high symmetry are, although also non-diffractive, very sensitive to turbulence. Furthermore, Airy Ring Beams, a new type of accelerating self focusing beams, exhibits robustness even at strong turbulence. Our results agree with the theoretical work of Chu and Gu [References 2, 3, 4] who studied the propagation of various beams including Airy Beams in turbulence.

Future work involves the detailed study of the propagation of self-accelerating beams, such as Airy Ring Beams in the presence of turbulence. Furthermore, another propagation regime in absorptive scattering media will be studied.

Appendix A

Code of Matlab for turbulent medium for 1D propagation:

```matlab
%N=number of sampling points at s
N=400;
%M=number of sampling points at propagation distance ksi
M=100;

smax=20;
ksimax=1;

%values of the constants
%Cn=refractive index structure
%l0=inner scale
%L0=outer scale
Cn2=10^-18;
l0=10^-2;
L0=3;

%generation of pseudorandom complex number
A1=randn(1,N);
B1=randn(1,N);
A=(A1+B1*1i);

%D=spatial sampling interval
D=2*smax/N; %0.1;

%Dk^-1=wave number increment
Dk=(2*pi)/(N*D);

K=linspace(0,10*pi/l0,N);

%karman type index power spectrum for the atmosphere turbulence
Fn=0.033*Cn2*exp((-

(K*l0)/(5.92*2*pi)).^2).*(((K/(2*pi)).^2+(1/(L0.^2))).^(-11/6));

%multipication with the random complex numbers
B=A.*Dk.*sqrt(Fn);

%B3=inverse fourier transform of B
B3=ifft(B);
B4=fftshift(B3,2);

%B5=the real part of the complex random phase field
B5=real(B4);
B1=max(max(B5));
B2=min(min(B5));

% normalized field
B5=((B5-B2)/(B1-B2))*2-1;

l=0.8*10^-6;
Dn=10^-4;
V=(4*pi/l)*Dn*B5;
```

Appendix B

Code of Matlab for 1+1D propagation of the Beam:

```matlab
function [fi]=beams

%N=number of sampling points at s
N=400;
%M=number of sampling points at propagation distance ksi
M=100;

ksimax=0.1;
smax=20;

m = 0;
s = linspace(-smax,smax,N);
ksi = linspace(0,ksimax,M);

sol = pdepe(m,@pdex1pde,@pdex1ic,@pdex1bc,s,ksi);
% extract the first solution component as fi
fi = sol(:,:,1);

function [c,f,s] = pdex1pde(s0,ksi0,fi,DfiDs)
c = -2*1i;
f = DfiDs;
% At s the disorder is introduced, for s=0, propagation is in vacuum
s = Dn.*fi;

% function pdex1ic is for the initial conditions
function u0 = pdex1ic(s)
%gaussian
u0 = exp(-(s)^2);

% %airy function
% a=0.1;
% u0 =airy(sqrt(2*log(2))*(2.28/2)*s)*exp(a*s);

% %airy ring function
% a=0.1;
% r0=2;
% w=0.466;
```

```matlab
% %u0 =1/airy(-1)*airy(2.28*s)*exp(2.28*a*s);

% u0 =(airy((s+r0)/w)+airy((r0-s)/w))*exp(-a*abs(s));


% function pdex1bc is for periodical boundary conditions
function [pl,ql,pr,qr] = pdex1bc(sl,fil,sr,fir,ksi)
pl = fil;
ql = 0;
pr = fil;
qr = 0;
```

Appendix C

Code of Matlab for turbulent medium for 2D propagation:

```matlab
%N=number of sampling points at s
N=512;
%M=number of sampling points at propagation distance ksi
M=10;


smax=0.325;


%D=spatial sampling interval
D=2*smax/N;


%l=wavelength
lamda=0.8*10^-6;
%k0=wavenumber
k0=(2*pi)/lamda;


%values of the constants
%Cn=refractive index structure
%l0=inner scale
%L0=outer scale
Cn2=10^-18;
l0=10^-2;
L0=5;


%generation of pseudorandom complex number
A1=2*((rand(N,N))-0.5);
B1=2*((rand(N,N))-0.5);
A=(A1+B1*1i);


chess=zeros(N,N);
for i=1:N
    for j=1:N
chess(i,j)=(-1)^(i+j);
    end
end


%Dk^-1=wave number increment
Dk=(2*pi)/(N*D);
```

```matlab
k1=linspace(-pi/D,pi/D,N);
k2=-linspace(-pi/D,pi/D,N);


[K1,K2] = meshgrid(k1,k2);
[~,r]=cart2pol(K1,K2);
K=r;
```

%karman type index power spectrum for the atmosphere turbulence
```matlab
Fn=0.033*Cn2*exp((-
(K*l0)/(5.92*2*pi)).^2).*(((K/(2*pi)).^2+(1/(L0.^2))).^(-11/6));
```

%Z=propagation dinstance
%dz=screen seperation for M random screens
```matlab
Z=10^3;
dz=Z/M;
```

%Ftheta=random phase power spectrum
```matlab
Ftheta=2*pi*(k0.^2).*dz.*Fn;
```

%multipication with the random complex numbers
```matlab
B=A.*Dk.*sqrt(Ftheta);
```

%B3=inverse fourier transform of B
```matlab
B3=ifft2(B,N,N)*(N^2);
```

%B4=the real part of the complex random phase field
```matlab
B4=real(B3).*chess;
```

Appendix D

Code of Matlab for 2+1D propagation in turbulence:

```
%N1=number of sampling points at s
N1=512;
%N2=number of sampling points at h
N2=512;
%M=number of sampling points at propagation distance ksi
M=10;


%l=wavelength
lamda=0.8*10^-6;
%k0=wavenumber
k0=(2*pi)/lamda;


smax=0.325;
hmax=0.325;
ksimax=1;


%ds=step size of s
ds=2*smax/N1;
%dh=step size of h
dh=2*hmax/N2;
%Z=total distance of z
Z=10^3;
%dz=step size of z
dz=Z/M;
s=linspace(-smax,smax,N1);
h=linspace(-hmax,hmax,N2);
Ks=linspace(-(pi*N1)/(2*smax),(pi*N1)/(2*smax),N1);
Kh=linspace(-(pi*N2)/(2*hmax),(pi*N2)/(2*hmax),N2);


%initial gaussian beam
%w0=waist of the beam
w0=50*10^-3;
[S H]=meshgrid(s,h);
[KS KH]=meshgrid(Ks,Kh);
beam_in=exp((-((S).^2)-((H).^2))/w0^2);


% %initial airy beam
```

```matlab
% %w0=waist of the beam
% w0=50*10^-3;
% t=0.128;
% [S H]=meshgrid(s-t,h-t);
% [KS KH]=meshgrid(Ks,Kh);
% a=0.05;
%beam_in=airy((S)/w0).*exp(a*(S)/w0).*airy((H)/w0).*exp(a*(H)/w0);


% %initial bessel beam
% [S,H] = meshgrid(s,h);
% [KS KH]=meshgrid(Ks,Kh);
% [~,r]=cart2pol(S,H);
% width=50*10^-3;
% P=r;
% beam_in=besselj(0,1.52114*(P/width));


% %initial beam airy ring
% [S,H] = meshgrid(s,h);
% [KS KH]=meshgrid(Ks,Kh);
% [~,r]=cart2pol(S,H);
% P=r;
% a=0.05;
% r0=50*10^-3;
% w=4.85*10^-3;
% beam_in =airy((r0-P)/w).*exp(a*((r0-P)/w));



% % plane wave
% [S H]=meshgrid(s,h);
% [KS KH]=meshgrid(Ks,Kh);
% beam_in=1;


%normalization of the beam
beam_in=beam_in/max(max(beam_in));


%free space transfer function of propagation
T=exp(-(1i*lamda/(4*pi))*dz*(KS.^2+KH.^2));


for z=0:dz:Z
% load the random phase screen
% Convert from k space to real space (generate theta)
```

```matlab
head='othoni';
Index=floor(z/dz)+1+100*i;
load ([head num2str(Index) '.mat']);


% Multiply current field with .*exp(1i*theta)
beam_in=beam_in.*exp(1i*V);


%gaussian beam in frequency domain
Fbeam=fft2(beam_in);


%propagated gaussian beam in frequency domain
Fbeam2=fftshift(Fbeam).*T;


%propagated gaussian in space domain
Beam=ifft2(fftshift(Fbeam2));


beam_in=Beam;
beam_in=beam_in/max(max(beam_in));
end
```

Appendix E

There are two different ways for computing scintillation index:

The first one will be mentioned as Scintillation Index over Space [Reference] and the second one as Scintillation Index over Time [Reference]. The Scintillation Index over Time refers to the variation of the signal intensity as a function of time and is directly correlated to the value one would measure in an experiment or application. The numerical estimation of this value is rather computationally intensive since it requires the repetition of the numerical propagation for several sets (typically more than 50) of random media. The intensity variation over time actually originates from the amount of "deformation" of the intensity profile caused by the turbulent medium. Taking this into account an alternative, less computationally intensive, scintillation index (over space) has been used [reference] to analyze simulation experiments. To estimate the Scintillation Index over Space one needs only one propagation simulation trough the turbulent medium. A similar to eq.63 is still used with the difference that averaging is preformed over space and not over time. So Scintillation over space actually "measures" the amount of beam deformation and can provide a much simpler measure of the effect of turbulence. Since the results in this case strongly depend on the intensity distribution of the unperturbed beam this index it can be safely used in tha case of plane waves and in small areas where the intensity is practically constant for more complex intensity profiles.

In Fig. 37 we compare the results from the simulation using two methods of Scintillation index evaluation σ_I^2 as function of the diameter of the detector for weak turbulence (for $C_n^2 = 10^{-18}$) for a Gaussian beam ($w_0 = 5cm$). The values of σ_I^2 are divided by their maximum value in order to be compared. As the diameter of the detector increases, Scintillation Index over space increases since it is affected by the intensity distribution of the Gaussian beam. In contrast, the Scintillation index σ_I^2 evaluated over time, decreases, as expected, as the detector diameter increases. These results clearly show that for the case of beams used in this work the scintillation over time is more accurate to use, while the scintillation over space is safe to use only with small detector diameters.
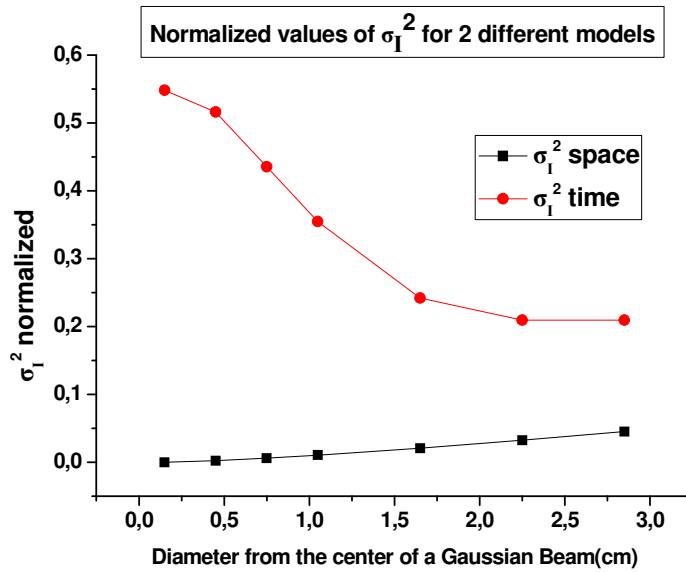
Figure 37: Comparison of 2 methods for computing SI (Scintillation Index), values of SI are normalized and computed as a function of the detector size (0.45cm).

The method of Scintillation Index over Time was used through all simulations.

Experimental values of scintillation index can be calculated with 2 ways [Reference]. The first one by using an aperture averaging setup and the second one by using a scintillometer setup (Figure 38). The two signals pass from an amplifier and the received signals are show in Figure 39. The first signal is detected by a scintillometer setup and the second signal by an aperture averaging receiver. It is shown that the second signal has smaller intensity fluctuations.
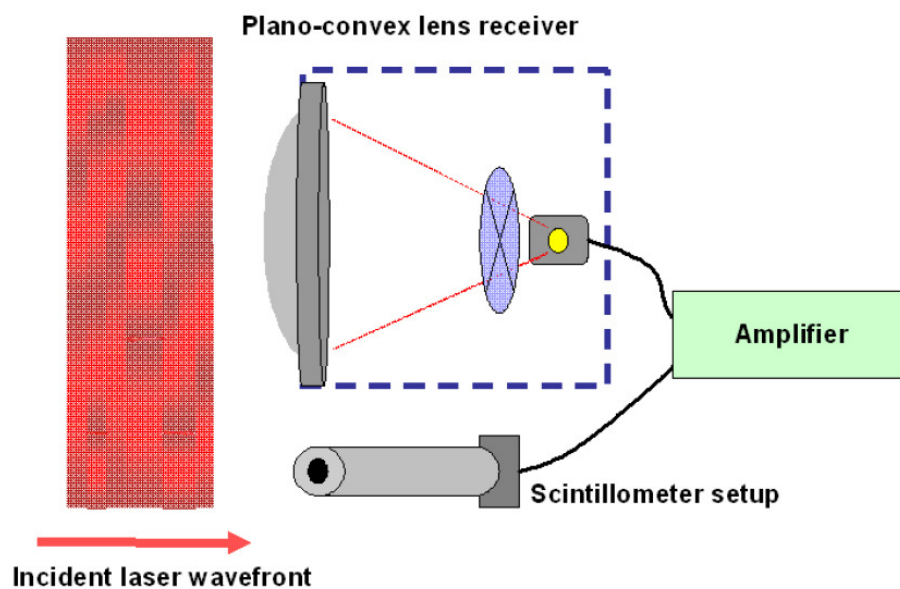

Figure 38: Diagram of the aperture averaging receiver setup and scintillometer setup
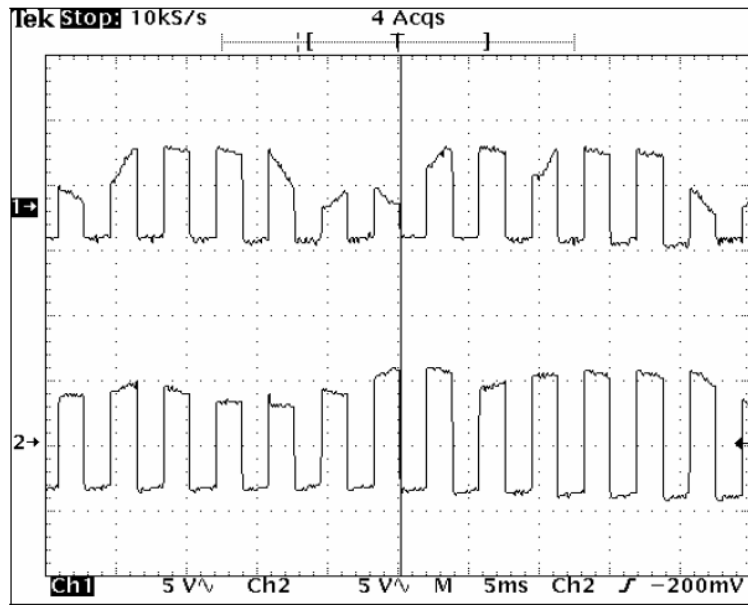
Figure 39: Channel 1: Optically chopped signal detected by the scintillometer. Channel 2: Optically chopped signal detected by the aperture averaged receiver

BIBLIOGRAPHY

[1] Xiaoming Zhu, Joseph M. Kahn, "Free-Space Optical Communications Through Atmospheric Turbulence Channels". IEEE Transactions on Communications, Vol. 50, No. 8, August 2002, p.: 1293-1300.

[2] Xiuxiang Chu, *"Evolution of Airy beam in turbulence"*. Optics Letters, Vol. 36, No. 14, 15 July 2011, p.: 2701-2703.

[3] Yalong Gu, Greg Gbur, *"Scintillation of Airy beam arrays in atmospheric turbulence"*. Optics Letters, Vol. 35, No. 20, 15 October 2010, p.: 3456-3458.

[4] Yalong Gu, Greg Gbur, *"Scintillation of pseudo-Bessel correlated beams in atmospheric turbulence"*. J. Opt. Soc. Am. A, Vol. 27, No. 12, December 2010, p.: 2621-2629.

[5] Nikolaos K. Efremidis, Jared Hudock, Demetrios N. Christodoulides, Jason W. Fleischer, "Two-Dimensional Optical Lattice Solitons". Physical Review Letters, Vol. 91, No. 21, 21 November 2003, p.:21306-1-213606-4.

[6] R. W. Ziolkowski, J. B. Judkins, *"Propagation characteristics of ultrawide-bandwidth pulsed Gaussian beams"*. J. Opt. Soc. Amer. A, Vol. 9, No.11, November 1992, p.: 2021-2030.

[7] Eugene Hecht, *"Optics"*, 4th edition. Addison Wesley, San Francisco, 2002, p.: 104-106.

[8] J. Durnin, J. J. Miceli, J. H. Eberly, *"Diffraction Free Beams"*. Physical Review Letters, Vol. 58, No. 15, 13 April 1987, p.: 1499-1501.

[9] J. Durnin, *"Exact solutions for nondiffracting beams. I. The scalar theory"*. J. Opt. Soc. Amer. A, Vol. 4, No.4, April 1987, p.: 651-654.

[10] G. A. Siviloglou, J. Broky, A. Dogariu, D. N. Christodoulides, *"Observation of Accelerating Airy Beams"*. Physical Review Letters, Vol 99, 20 November 2007, p.: 213901-213901.

[11] Georgios A. Siviloglou, Demetrios N. Christodoulides, *"Acceleration finite energy Airy beams"*. Optics Letters, Vol. 32, No. 8, 15 April 2007, p.: 979-981.

[12] M. V. Berry, N.L. Balazs, *"Nonspreading wave packets"*. Am. J. Phys., Vol. 47, No.3, March 1979, p.: 264-267

[13] Nikolaos K. Efremidis, Demetrios N. Christodoulides, *"Abruptly autofocusing waves"*. Optics Letters, Vol. 35, No. 23, 1 December 2010, p.: 4045-4047.

[14] Dimitrios G. Papazoglou, Nikolaos K. Efremidis, Demetrios Christodoulides, Stelios Tzortzakis, *"Observation of abruptly autofocusing waves"*. Optics Letters, Vol. 36, No. 10, 15 May 2011, p.: 1842-1844.

[15] V. E. Zuev (ed.), *"Laser Beams in the Atmosphere"*. Consultants Bureau, New York, 1982, p.: 189-192.

[16] Linda Marie Wasiczko, Dissertation directed by Professor Christopher C. Davis Department of Computer Engineering with title *"Techniques to mitigate the effects of atmospheric turbulence on free space optical communication links"*.

[17] V. I. Tatarskii, A. Ishimaru, V. U. Zavorotny (editors), *"Wave Propagation in Random Media (Scintillation)"*, Invited papers of a conference held 3-7 August 1992, University of Washington, Seattle, Washington. V.I Tatarskii, "Review of scintillation Phenomena".

[18] Herve Trinquet, Jean Vernin, *"Using meteorological forecasts to predict astronomical 'seeing'"*. Newsroom, SPIE 2009, 10.1117/2.1200906.1704

[19] http://www.handprint.com/ASTRO/seeing1.hml

[20] A. Ishimaru, *"Wave Propagation and Scattering in Random Media"*. IEEE Press (1997), p.: 57-70.

[21] A. Dipankar, P. Sagaut, *"A new phase-screen method for electromagnetic wave propagation in turbulent flows using large-eddy simulation"*. Journal of Computational Physics, Vol. 228, July 2009, p.: 7729-7741.

[22] Aniceto Belmonte, "Feasibility study for the simulation of beam propagation: consideration of coherent lidar performance". Applied Optics, Vol. 39, No. 30, 20 October 2000, p.: 5426-5445.

[23] Xianhe Liu, Jixiong Pu, *"Investigation on the scintillation reduction of elliptical vortex beams propagating in atmospheric turbulence"*. Optics Express, Vol. 19, No. 27, 19 December 2011,p.: 26444-26450

[24] J. M. Martin, Stanley M. Flatte, *"Intensity images and statistics from numerical simulation of wave propagation in 3-D random media"*. Applied Optics, Vol. 27, No. 11, 1 June 1988,p.: 2111-2126.

[25] J. M. Martin, Stanley M. Flatte, *"Simulation of point-source scintillation through three-dimensional random media"*. J. Opt. Soc. Am. A, Vol. 7, No. 5, May 1990, p.: 838-847.

[26] Joseph W. Goodman, *"Introduction to Fourier Optics"*. The McGraw-Hill Companies, Second Edition, (1996), Chapter 3.10, p.: 55-61.

[27] L. C. Andrews, M. A. Al-Habash, C. Y. Hopen, R. L. Phillips, *"Theory of optical scintillation: Gaussian-beam wave model"*. Waves In Random Media, Vol. 11, April 2001, p.: 271-291